

# REGISTRATION OF MULTIPLE SHAPES USING CONSTRAINED OPTIMAL CONTROL

SYLVAIN ARGUILLÈRE, EMMANUEL TRÉLAT, ALAIN TROUVÉ, AND LAURENT YOUNES

**ABSTRACT.** Lagrangian particle formulations of the large deformation diffeomorphic metric mapping algorithm (LDDMM) only allow for the study of a single shape. In this paper, we introduce and discuss both a theoretical and practical setting for the simultaneous study of multiple shapes that are either stitched to one another or slide along a submanifold. The method is described within the optimal control formalism, and optimality conditions are given, together with the equations that are needed to implement augmented Lagrangian methods. Experimental results are provided for stitched and sliding surfaces.

## 1. INTRODUCTION

The large deformation diffeomorphic metric mapping (LDDMM) approach to shape matching is a powerful topology-preserving registration method with an increasing record of successful applications in medical imaging. It was first described in [38] for point sets and in [17, 61, 46, 8] for images, and has become widely used in the medical imaging literature and other applications. While deeper understanding and extensions of the underlying theoretical framework was pursued [47, 22, 10, 48, 72, 21, 73, 9, 2] and alternative numerical methods were designed [5, 14, 62, 50, 29, 66, 4, 28, 18], LDDMM has been applied to medical imaging data including brain [45, 79, 53, 11, 56], heart [1, 6] and lung [58, 55, 52, 67] images. This algorithm provides a non-rigid registration method between various types of objects (point sets, curves surfaces, functions, vector fields. . .) within a unified framework driven by Grenander's concept of deformable templates [25]. It optimizes a flow of diffeomorphisms that transform an initial object (shape) into a target one.

The practical importance of shape registration is underlined by the increasing amount of work that has flourished in the literature over the past few years. LDDMM is one among many methods that have been proposed to perform this task. Several such methods are based on elastic matching energies [7, 16], and other, like LDDMM, inspired by viscous fluid dynamics [12, 59, 64, 3, 65, 49]. For surfaces, which will be our main focus, several authors have developed approaches to find approximate conformal parametrizations with respect to the unit disk or sphere [33, 31, 36, 26, 37, 70, 34, 27, 35]. More recently, quasi-conformal parametrizations based on the minimization of the Beltrami coefficient have been designed [77, 41, 69]. Another class of non-rigid registration methods include those based on optimal mass transportation [30, 32, 39, 40], while [44, 42, 43] introduce comparison methods based on Gromov–Hausdorff or Gromov–Wasserstein distances. Computational methods based on integer programming and graph optimization have also been recently introduced [78, 80, 23]. We also refer the reader to the survey papers [81, 15, 71, 74] and textbooks [24, 73] for additional entries on the literature.

In this paper, we discuss an extension of the LDDMM framework, in which multiple shapes are registered simultaneously within a deformation scheme involving—in a restricted form—contact constraints among the shapes. This is represented and solved as a constrained optimal control problem, in the spirit of the general framework recently introduced in [2].

Indeed, one of the characteristics of LDDMM is that it derives shape deformation from a global diffeomorphisms of the whole ambient space considered as a homogeneous medium, and does not allow for a differentiation of the deformation properties assumed by the shapes, or, more precisely, the objects they represent. This crude modeling may

---

2000 *Mathematics Subject Classification.* 58D05 49N90 49Q10 68E10.

*Key words and phrases.* Shape analysis; optimal control; deformations; groups of diffeomorphisms.

This work was partially supported by the ONR N000140810606 and by NSF 1335035.

provide results that are not realistic in some applications. Consider the situation in which one studies several shapes, representing, for example, different sub-structures of the brain. In this case, if one assumes that all shapes are deformed by a single flow of diffeomorphisms, shapes coming too close to one another will undergo a tremendous deformation, which creates artifacts that can mislead subsequent analyses. One would rather associate a different diffeomorphism to each shape, independent from the others, but the issue is that the resulting collection of diffeomorphisms may not be consistent: the shapes could overlap along the deformation. The solution briefly introduced in [2] and developed in this paper is the following: embed the shapes into a "background", complement of the shapes, deformed by a new, independent deformation, and add *constraints* such that, as all the shapes are simultaneously transformed, their boundary moves with the boundary of the background so that the configuration consistency is preserved. This is the approach that we develop here, focusing on surface registration. Note that a multi-diffeomorphism approach has been recently developed for image matching [57], each diffeomorphism being restricted to a fixed region of the plane. The main (and fundamental) contrast with what we develop here is that, in our case, these subregions are variable and optimized, while they were fixed in [57]. The models along which sliding constraints are addressed in this paper and ours also differ. Certain approaches for sliding images have been investigated in [58, 55, 52] without the LDDMM viewpoint.

This paper is organized as follows. We start by recalling the classical LDDMM algorithm in Section 2, setting the definitions, notation and appropriate framework for the rest of the paper. Then, in Section 3, we introduce rigorously the concept of multishape, describe identity and sliding background constraints, and describe the augmented Lagrangian algorithm for general constraints that will be used for in our numerical simulations. Section 4 follows, specializing the algorithm to the case of identity and sliding constraints in great details. Finally, Section 6 applies our method to synthetic examples to real data as well.

## 2. LARGE DEFORMATION DIFFEOMORPHIC METRIC MAPPING

**2.1. Notation.** Throughout the paper, for any Banach space  $X$ , the notation  $(\mu|v)$  will be used to designate the application  $\mu(v)$  of a linear form  $\mu \in X^*$  to a vector  $v \in X$ .

We define a *shape* as a  $C^p$  embedding  $q : M \rightarrow \mathbb{R}^d$ , where  $M$  is a compact manifold and  $p$  is a positive integer. We denote by  $\mathcal{M}$  the corresponding *shape space* (the space of all such embeddings), which is an open subset of the Banach space  $\mathcal{Q} = C^p(M, \mathbb{R}^d)$ .

Typical examples are as follows:

- $M = \{1, \dots, l\}$  is finite, and  $q$  can be identified with a collection  $x_1, \dots, x_l$  of distinct points in  $\mathbb{R}^d$ .
- $M = [0, 1]$  and  $q$  is a curve in  $\mathbb{R}^d$ .
- $M = S^{d-1}$  (the unit sphere in  $\mathbb{R}^d$ ) and  $q$  is a hypersurface.

In practice, continuous shapes need to be discretized, for example with a triangulation, making the first case the most important.

Our goal is to discuss models in which several shapes can deform, while being subject to contact constraints. The deformation process will be similar to the one designed for *large deformation diffeomorphic metric mapping* (LDDMM), which can be formulated as an *optimal control problem*. Before introducing our general framework, it will be easier to start with a description of the now well explored single-shape problem upon which we will build. For this, we let  $(V, \|\cdot\|_V)$  be a Hilbert space of vector fields on  $\mathbb{R}^d$ , assumed to be continuously embedded in the Banach space  $C_0^p(\mathbb{R}^d, \mathbb{R}^d)$  of vector fields on  $\mathbb{R}^d$  going to 0 at infinity (that is, the completion of the space of smooth compactly supported vector fields for the norm  $\|\cdot\|_{p,\infty}$ , which denotes the sum of supremum norms of derivatives of order  $p$  or less, with  $p \geq 1$ ). Then  $V$  possesses a *reproducing kernel*: a mapping  $K : (x, y) \in (\mathbb{R}^d)^2 \mapsto K(x, y) \in M_d(\mathbb{R})$ , where  $M_d(\mathbb{R})$  denotes the space of  $d \times d$  matrices, such that

$$K(\cdot, y)a \in V \quad \text{with} \quad \langle K(\cdot, y)a, w \rangle_V = a \cdot w(y),$$

for all  $(a, y) \in (\mathbb{R}^d)^2$  and  $w \in V$ . Moreover, all partial derivatives with order at most  $p$  with respect to each variable exist. The LDDMM algorithm uses flows of time-dependent vector fields  $v(\cdot) \in L^2(0, 1; V)$  with square-integrable norms in  $V$  with respect to time.

In practice, one usually uses radial kernels, that is, kernels of the form  $K(x, y) = G(\frac{|x-y|^2}{\sigma})\text{Id}_{\mathbb{R}^d}$ , with  $G : \mathbb{R}^+ \rightarrow [0, 1]$  a smooth decreasing function. The positive number  $\sigma$  is called the *scale* of the kernel.

## 2.2. Registering Two Shapes Using LDDMM.

*General Problem.* The general LDDMM problem is formulated as the infinite-dimensional optimal control problem consisting of minimizing the cost functional

$$(1) \quad \tilde{F}(v) = \frac{1}{2} \int_0^1 \|v(t)\|_V^2 dt + U(q(1)),$$

subject to the constraint

$$(2) \quad \begin{aligned} \partial_t q(t) &= v(t) \circ q(t) \quad \text{for a.e. } t \in [0, 1], \\ q(0) &= q_{init}. \end{aligned}$$

This differential constraint gives a control system, where the control is the time-dependent vector field  $v(\cdot) \in L^2(0, 1; V)$ , the solution of which is  $q(t) = \varphi(t) \circ q_{init}$  with  $\varphi$  is the flow of diffeomorphisms generated by  $v(\cdot)$ . Recall that this flow is defined as the unique solution of the Cauchy problem  $\partial_t \varphi(t) = u(t) \circ \varphi(t)$ ,  $\varphi(0) = \text{id}_{\mathbb{R}^d}$ . For every time  $t$ , we have  $\varphi(t, \cdot) \in \text{Diff}^p$ , the set of  $p$ -times differentiable diffeomorphisms in  $\mathbb{R}^d$ .

The function  $U : \mathcal{Q} \rightarrow \mathbb{R}$  is a matching cost function, that is, a penalization that pushes the solution of (1)-(2) towards a target. It will be assumed to be Fréchet differentiable from  $\mathcal{Q}$  to  $\mathbb{R}$ . To simplify the discussion, and because this covers most of the interesting cases in practice, we will assume that there exists some fixed measure  $\nu_M$  on  $M$  such that the derivative of  $U$ , denoted  $dU(q)$  or  $dU_q$  when evaluated at  $q \in \mathcal{Q}$ , can be expressed in the form  $dU_q = z_q \nu_M$  for some  $(\nu_M$ -measurable)  $z_q : M \rightarrow \mathbb{R}^d$ , that is,

$$\forall h \in \mathcal{C}^p(M, \mathbb{R}^d), \quad (dU_q | h) = \int_M h(m) \cdot z_q(m) d\nu_M(m).$$

In most cases,  $U$  is an  $L^2$ -norm, a measure norm or a current norm [63]. See Appendix A for more details. Under these assumptions, the cost  $\tilde{F}$  is Fréchet differentiable on the Hilbert space  $L^2(0, 1; V)$ , and its differential can be computed explicitly.

*Derivative of a Cost Functional in Optimal Control: Hamiltonian Formulation.* We briefly recall the method for the computation of the derivative of a cost functional in the framework of control theory. We refer to [2] or [60] for details, and just give the result. Consider a Hilbert space  $V$  and a Banach space  $B$ , a fixed point  $x_0 \in B$ , functions  $L : B \times V \rightarrow \mathbb{R}$  and  $g : B \rightarrow \mathbb{R}$ , a mapping  $f : B \times V \rightarrow B$ , and a cost function of the form

$$E(u) = \int_0^1 L(x(t), u(t)) dt + g(x(1)),$$

where the control  $u$  belongs to  $L^2(0, 1; V)$ , and  $x : [0, 1] \rightarrow B$  is the solution of the Cauchy problem  $x(0) = x_0$  and

$$\dot{x} = f(x, u)$$

almost everywhere. Then, assuming  $L, g$  and  $f$  are of class  $\mathcal{C}^1$  and the Fréchet derivative of  $\partial_u L(x, u)$  in  $u$  is bounded by a continuous function of  $(x, u)$  that has linear growth as  $u$  goes to infinity,  $E$  is differentiable. This derivative can be computed using the *Hamiltonian*  $H : B \times B^* \times V \rightarrow \mathbb{R}$  of the system, defined by  $H(q, p, u) = (p | f(q, u)) - L(q, u)$ . Now, for a fixed control  $u$  and trajectory  $x$ , an integration by part shows that

$$\forall \tilde{u} \in L^2(0, 1; V), \quad (dE_u | \tilde{u}) = - \int_0^1 (\partial_u H(q(t), p(t), u(t)) | \tilde{u}(t)) dt,$$

where the *costate*  $p : [0, 1] \rightarrow B^*$  is the solution of the Cauchy problem  $p(1) = -dg(x(1))$  and  $\dot{p}(t) = -\partial_x H(x(t), p(t), u(t))$  for almost every  $t$  in  $[0, 1]$ .

Now, applying this method to our framework, we see that the Hamiltonian is given by  $(p|v \circ q) - \frac{1}{2}\|v\|^2$ . From there, we easily get that, for  $p : [0, 1] \times M \rightarrow \mathbb{R}^d$  be the solution of the Cauchy problem  $p(1) = -z_{q(1)}$  (so that  $dU_{q(1)} = p(1) d\nu_M$ ), and  $\partial_t p = -(dv \circ q)^T p$ , we have

$$\forall X \in L^2(0, 1; V), \quad (dF_v|X) = \int_0^1 \langle v(t), X(t) \rangle_V dt - \int_0^1 \int_M X(t, q(t, m)) \cdot p(t, m) d\nu_M(m) dt.$$

The properties of the reproducing kernel then yields

$$(dF_v|X) = \int_0^1 \left\langle v(t) - \int_M K(\cdot, q(t, m)) p(t, m) d\nu_M(m), X(t) \right\rangle_V dt.$$

We deduce the gradient  $\nabla \tilde{F}(v)$  of  $\tilde{F}$  at  $v$  in  $L^2(0, 1; V)$  for its canonical Hilbert product. It is the time-dependent vector field satisfying, for almost every  $t \in [0, 1]$ , and every  $x \in \mathbb{R}^d$ ,

$$(3) \quad \nabla \tilde{F}(v)(t, x) = v(t, x) - \int_M K(x, q(t, m)) p(t, m) d\nu_M(m).$$

*Reduced Problem.* An optimal control  $v$  must satisfy  $\nabla F(v) = 0$ . Hence, there exists  $\alpha : M \rightarrow \mathbb{R}^d$  such that for almost every  $t$  in  $[0, 1]$  and every  $x$  in  $\mathbb{R}^d$ ,

$$(4) \quad v(t, x) = \int_M K(x, q(t, m)) \alpha(t, m) d\nu_M(m)$$

for some function  $\alpha : [0, 1] \times M \rightarrow \mathbb{R}^d$ . It is therefore natural to parametrize  $v$  by  $\alpha$  and use this function as a new control. Now, for  $q$  in  $\mathcal{Q}$  fixed, we define the inner product

$$\langle \alpha, \beta \rangle_q = \int_{M \times M} \alpha(m) \cdot K(q(m), q(\tilde{m})) \beta(\tilde{m}) d\nu_M(m) d\nu_M(\tilde{m})$$

between two measurable  $\mathbb{R}^d$ -valued functions  $\alpha$  and  $\beta$  defined on  $M$ . If  $v$  is given by (4), the reproducing property of the kernel implies that  $\|v\|_V^2 = \|\alpha\|_q^2$ . The optimal control problem (1)-(2) is then equivalent to the reduced problem consisting of minimizing the cost functional

$$(5) \quad F(\alpha) = \frac{1}{2} \int_0^1 \|\alpha(t)\|_{q(t)}^2 dt + U(q(1)),$$

subject to the constraint (control system)

$$(6) \quad \partial_t q(t, m) = \int_M K(q(t, m), q(t, \tilde{m})) \alpha(t, \tilde{m}) d\nu_M(\tilde{m}),$$

almost everywhere over the time interval  $[0, 1]$ . When  $M = \{1, \dots, l\}$  is a finite set, we have  $\alpha : [0, 1] \rightarrow \mathbb{R}^d$ , so this formulation drastically reduces the type of controls to consider. According to [6, 13, 63, 75] (or just using the same method as above), the gradient of  $F$  with respect to the inner product  $\langle \cdot, \cdot \rangle_q$  is

$$\nabla F(\alpha) = \alpha - p,$$

where  $p$  is a time-dependent vector-valued measurable function on  $M$  such that  $p(1)\nu_M = -dU_{q(1)}$  and

$$\partial_t p(t) = -\partial_q \left( \langle p(t), \alpha(t) \rangle_q - \|\alpha(t)\|_{q(t)}^2 / 2 \right).$$

### 3. MULTIPLE SHAPE PROBLEMS

**3.1. Motivating Examples.** In the previous formulation, the shape evolution was controlled by a single, smooth vector field  $v$ , inducing a single diffeomorphism of  $\mathbb{R}^d$  restricted to the considered shape. This approach has been successfully used to model variations of single, homogeneous shapes, and led to important applications in computational anatomy, including, among many other examples, the impact of pathologies like Huntington disease [76], schizophrenia [54], and Alzheimer’s disease [68, 19, 56] on brain structures. This deformation model, however, is not well adapted in situations in which several shapes interact, or situations in which shapes have heterogeneous parts.

More precisely, it is natural, when analyzing multiple organs in the human body, to consider multiple shapes, each of them corresponding to a different organ, being relatively stable (only subject to small deformations) while their position with respect to each other is subject to larger variations, so that the background (the intersection of their complements) undergoes very large deformations (see Figure 1). This is not possible with the classical LDDMM method. With this new model, the shapes would never come into contact, but they would only interact when they come very close to one another, and only in such a way as to not overlap. One can see this as an approximation of a contact problem [58, 55, 52].

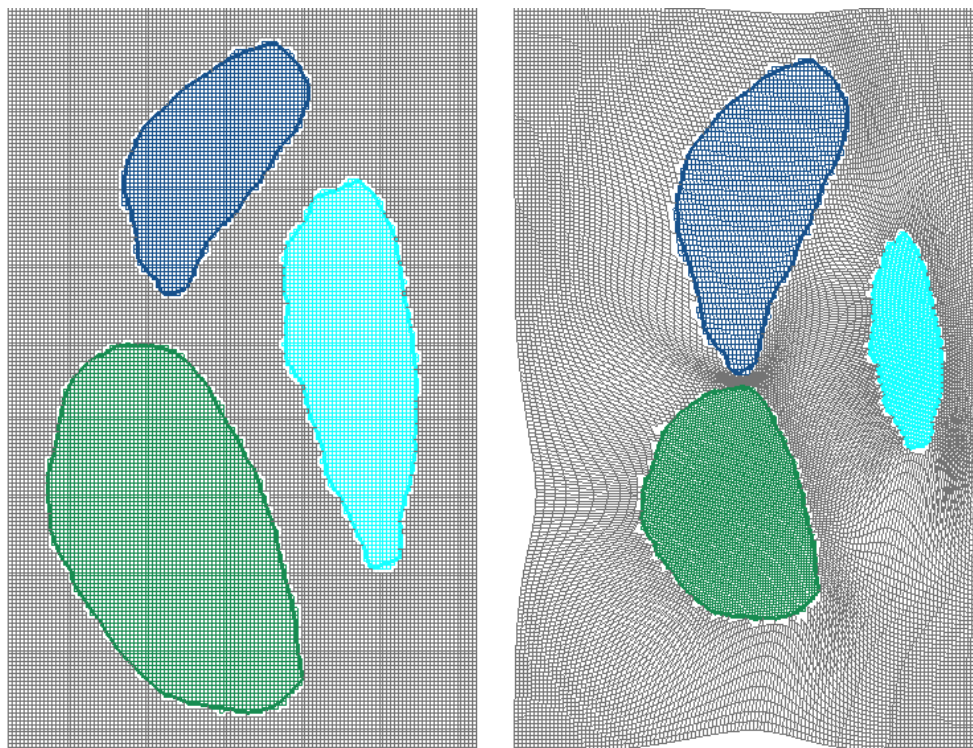


FIGURE 1. Each colored area represents a different organ, and undergoes a small and very smooth deformation, while the background is subject to much larger variations.

This suggests using multiple components to describe a shape, and multiple deformations applied separately to each component of the considered model. Generalizing (1)-(2), consider parameter spaces  $M_1, \dots, M_n$  for an  $n$ -component model. Each shape, or component, is a mapping  $q^{(k)} \in \mathcal{Q}_k$  the space of embeddings of  $M_k$  in  $\mathbb{R}^d$  of class  $\mathcal{C}^p$ . The space of states will then be  $\mathcal{Q} = \mathcal{Q}_1 \times \dots \times \mathcal{Q}_n$ . To each shape, associate a control  $v_k \in V_k$ , where  $V_k$  is an RKHS

embedded in  $C_0^p(\mathbb{R}^d, \mathbb{R}^d)$  with the state evolution equation  $\partial_t q^{(k)} = v_k \circ q^{(k)}$ . We can then choose each  $V_k$  according to how “wildly” we want to allow the  $k$ -th shape to deform.

These evolutions, however, must be consistent with each other, implying certain contact constraints. We will consider two forms of such constraints:

- **Identity constraints:** These are constraints that make a subset of the  $k$ -th shape stay stitched to a subset of the  $l$ -th shape, so that these subsets coincide in  $\mathbb{R}^d$  and move identically along the deformation. In other words, given some pair  $(k, l) \in \{1, \dots, n\}^2$ , and given a one-to-one mapping  $g_{kl} : A_{kl} \subset M_k \rightarrow A_{lk} = g_{kl}(A_{kl}) \subset M_l$ , one has  $q^{(k)}(x) = q^{(l)}(g_{kl}(x))$  for every  $x \in A_{kl}$ .
- **Sliding constraints:** These are constraints that force a closed submanifold of the  $k$ -th shape to slide on a corresponding submanifold of the  $l$ -th shape along the deformation, for all  $(k, l)$ . Here, we assume that all parameter spaces are orientable differential manifolds, and that all  $q^{(k)}$ 's are immersions. Given some pair  $(k, l) \in \{1, \dots, n\}$ , and a closed submanifold without boundary  $A_{kl} \subset M_k$ , there exists a diffeomorphism  $g_{kl} : A_{kl} \rightarrow A_{lk} \subset M_l$  onto a fixed closed submanifold  $A_{lk}$  of  $M_l$  such that  $q^{(k)}(x) = q^{(l)}(g_{kl}(x))$  for every  $x \in A_{kl}$ .

Let us give some quick examples. Consider a schematic representation of a kite, or a manta ray, composed with a two-dimensional surface, representing the body, and an open curve attached to it representing the tail. When comparing two such objects, the body is assumed to only show small differences in shape, while the tail can vary widely. This leads us to take  $M_1 = S^2$  and  $M_2 = [0, 1]$ , and, letting  $m_0$  represent the north pole in  $S^2$ , impose the contact point  $q^{(1)}(m_0) = q^{(2)}(0)$ . We can then assign different deformation models to  $q^{(1)}$  and  $q^{(2)}$  via the metrics on  $V_1$  and  $V_2$ .

Now for studying  $n - 1$  organs simultaneously, which is our main goal, we need  $n$  shapes,  $n - 1$  of which are associated with the organs, and the last of which represents the background, the medium in which the organs evolve. For example, we can take  $M_k = S^2$ , the sphere in  $\mathbb{R}^3$ , for  $k = 1, \dots, n - 1$ , and  $M_n = \{1, \dots, n - 1\} \times S^2$ . Then, to ensure that the shapes do not intersect, we can define identity or sliding constraints for the background, enforcing  $q^{(n)}(k, \cdot) = q^{(k)}(\cdot)$  or  $q^{(n)}(\{k\} \times S^2) = q^{(k)}(S^2)$  for  $k \in \{1, \dots, n - 1\}$  during the deformation. Consequently, while each shape evolves independently from the others, their movement must coincide with that of the background, and therefore they cannot intersect. We can then choose a kernel space  $V_n$  inducing the background transformation that allows larger variations. Figure 1 gives an example (in 2D) with 3 organs ( $n = 4$ ).

*Remarks on sliding constraints.* The sliding constraints described in this paper are rather restrictive. They require constant contact between certain submanifolds of each shape along the deformation. In particular, we do not consider collision or separation of shapes. This could theoretically be accomplished with certain inequality constraints, but the mathematical results (existence of optimal controls, first order optimality conditions) no longer hold for continuous shapes, while such constraints are very hard to model for triangulations and landmarks.

However, in the case of several shapes evolving in a background, both identity and sliding constraints can be considered as approximations of the collision and separation problem: the larger the deformation we allow on the background, the closer the shapes will need to be to interact.

**3.2. Induced Constraints on the Vector fields.** The constraints defined in the previous section are hard to take into account in a minimization algorithm. However, they can be reformulated as equality constraints involving the state and control in a way that is much more suitable to optimization.

Identity constraints  $q^{(k)}(x) = q^{(l)}(g(x))$  are equivalent (taking time derivatives) to  $v_k(t, q^{(k)}(t, x)) = v_l(t, q^{(l)}(t, g(x)))$  as soon as the constraints are satisfied at time  $t = 0$ , which we obviously assume.

Making the same assumption, sliding constraints simply mean that the normal part of the deformations coincide along the embedded constrained manifolds. This can be expressed as

$$(7) \quad N^{(k)}(t, q^{(k)}(t, m))^T (v_k(t, q^{(k)}(t, m)) - v_l(t, q^{(l)}(t, m))) = 0,$$

where  $N^{(k)}(t, q^{(k)})$  is a  $d \times (d - \dim(A_{kl}))$  matrix consisting of independent vectors perpendicular to  $T_{q^{(k)}} B_{kl}(t)$  (e.g, a normal frame to  $B_{kl}$ ), with  $B_{kl} = q^{(k)}(A_{kl})$  for every  $(k, l)$ . Do note how much easier this is to consider, partly

because it only depends on one of the shapes. This will also be useful when considering triangulations of the surfaces for practical applications. Let us briefly justify our statement.

We express the sliding constraint as  $q^{(k)}(t, m) = q^{(l)}(t, g(t, m))$  for some diffeomorphism  $g(t, \cdot) : A_{kl} \rightarrow A_{lk}$ , assuming a differentiable dependency on time. Taking time derivatives, we get

$$v_k(t, q^{(k)}(t, m)) = v_l(t, q^{(l)}(t, g(t, m))) + dq^{(l)}(t, g(t, m))\partial_t g(t, m), \quad m \in M_k.$$

Since  $q^{(l)}(t, g(t, m)) = q^{(k)}(t, m)$ , we obtain

$$\begin{aligned} v_k(t, q^{(k)}(t, m)) - v_l(t, q^{(k)}(t, m)) &= dq^{(l)}(t, g(t, m))\partial_t g(t, m) \\ &= dq^{(k)}(t, m)dg(t, m)^{-1}\partial_t g(t, m), \end{aligned}$$

which is tangent to  $B_{kl}$  at  $m$ . Note that, since the image of  $g(t, \cdot)$  is  $A_{lk}$  for every time  $t$ , we do have  $\partial_t g(t, m) \in T_{g(t, m)}A_{lk} = dg(t, m)(T_m A_{kl})$ , so  $dg(t, m)^{-1}\partial_t g(t, m)$  is well defined.

Conversely, assume that (7) holds for every  $x \in A_{kl}$ , with  $q^{(k)}(0, x) = q^{(l)}(0, g_0(x))$  for some diffeomorphism  $g_0 : A_{kl} \rightarrow A_{lk} \subset M_l$ . Then for every time  $t$ , the mapping

$$w : x \in A_{kl} \mapsto \underbrace{dq^{(k)}(t, x)^{-1}(v_k(t, q^{(k)}(t, x)) - v_l(t, q^{(k)}(t, x)))}_{\in T_{q^{(k)}(t, x)}B_{kl}} \in T_x A_{kl}$$

defines a time-dependent vector field on  $A_{kl}$ . Since  $A_{kl}$  is a closed manifold, this vector field is complete, and we denote its flow by  $h(t, \cdot) : A_{kl} \rightarrow A_{kl}$ . Then

$$\begin{aligned} \partial_t q^{(k)}(t, h(t, x)) &= v_k(t, q^{(k)}(t, h(t, x))) + dq^{(k)}(t, h(t, x))\partial_t h(t, x) \\ &= v_l(q^{(k)}(t, h(t, x))), \end{aligned}$$

where the last identity holds for every  $x \in A_{kl}$ , so that  $q^{(k)}(t, h(t, x))$  and  $q^{(l)}(t, g_0(x))$  satisfy the same differential equation with the same initial condition and therefore coincide. Hence, letting  $g(t, x) = g_0(h^{-1}(t, x))$ , we obtain  $q^{(l)}(t, g(t, x)) = q^{(k)}(t, x)$  for every  $x \in A_{kl}$ .

It is possible to extend this construction to the case where  $A_{kl}$  is a compact manifold with boundary. In this case, the matrix  $N^{(k)}(t)$  must consist of a normal frame along  $\partial B_{kl}(t)$  and possesses therefore an extra column, and we get an additional constraint along the boundary of  $A_{kl}$ .

We will need the constraints to depend smoothly on  $q$ , and therefore we will need a smooth representation of the normal space to  $q$  (a smooth map  $q \mapsto N(q)$ ) in order to be able to use (7). For this, we can introduce a new state  $N^{(k)}(t, x)$  evolving according to

$$(8) \quad \partial_t N^{(k)} = -dv_k(q^{(k)})^T N^{(k)},$$

such that, at time  $t = 0$ ,  $N^{(k)}(0, \cdot)$  is a normal frame along  $q^{(k)}(0)$ , which ensures that  $N^{(k)}(t, x)$  remains perpendicular to  $T_{q^{(k)}(t, x)}S_k$ . The constraint  $N^{(k)}(t, x)^T(v_k(t, q^{(k)}(t, x)) - v_l(t, q^{(k)}(t, x)))$  is now a smooth function of the extended state.

*Infinite dimensional minimization.* The two problems that we consider are special cases of the general problem considered in [2], which is the problem of minimizing a cost functional

$$(9) \quad \frac{1}{2} \sum_{k=1}^n \int_0^1 \|v_k(t)\|_{V_k}^2 dt + \sum_{k=1}^n U_k(q^{(k)}(1)),$$

subject to constraints of the form

$$(10) \quad \partial_t q^{(k)}(t) = v_k(t, q^{(k)}(t)), \quad \text{and} \quad C(q(t))v(t) = 0,$$

almost everywhere over the time interval  $[0, 1]$ , where  $C : \mathcal{M} \rightarrow L(V, \mathcal{Y})$  takes values in the space of bounded linear operators from  $V$  to a Banach space  $\mathcal{Y}$ . Here, we have  $V = V_1 \times \dots \times V_n$  and  $q = (q^{(1)}, \dots, q^{(n)})$ . Let us note that, according to [2, Theorem 1], there always exists at least one solution of (9)-(10) satisfying the constraints.

Our constrained optimization algorithm uses the augmented Lagrangian method (see, e.g., [51]). In a nutshell, in order to minimize a function  $u \mapsto F(u)$  subject to multi-dimensional equality constraints  $C(u) = 0$ , the augmented Lagrangian method consists in considering the functional

$$F_{\lambda,\mu}(u) = F(u) - (\lambda | C(u)) + \frac{\mu}{2}|C(u)|^2,$$

in which  $\lambda$  lives in the dual space of the space of constraints  $\mathcal{Y}$ , and  $\mu$  is a positive real number. Each iteration of the algorithm consists in minimizing  $F_{\lambda,\mu}$  with fixed  $\lambda$  and  $\mu$  (our implementation uses nonlinear conjugate gradient) until the gradient norm passes below some upper bound, and then in updating  $\lambda$  according to the rule

$$\lambda \leftarrow \lambda - \mu C(u),$$

before running a new minimization of  $F_{\lambda,\mu}$ , with updated values of  $\mu$  and  $\lambda$ . The constant  $\mu$  is increased only if needed, i.e., if the norm of the constraint did not decrease enough during the minimization. More details can be found in [51].

The study of this constrained optimal control problem, and in particular, the derivation of its first-order optimality conditions (of the type of the Pontryagin maximum principle), is challenging in this infinite-dimensional setting. In [2], it is proved that, under some differentiability conditions, and *under the important assumption that  $C(q)$  is surjective for every  $q \in \mathcal{M}$* , optimal solutions must be such that there exist  $p = (p^{(1)}, \dots, p^{(n)}) \in H^1([0, 1], \mathcal{Q}^*)$  and  $\lambda \in L^2([0, 1], \mathcal{Y}^*)$  that satisfy

$$(11) \quad \begin{cases} \partial_t q^{(k)} = v_k(q^{(k)}), \\ \partial_t p^{(k)} = -\partial_{q^{(k)}}(p^{(k)} | v_k(q^{(k)})) - \partial_{q^{(k)}}(\lambda | C(q)v), \\ \langle v_k, \tilde{v} \rangle_{V_k} = -\left(p^{(k)} | \tilde{v} \circ q^{(k)}\right) - (\lambda | C_k(q)\tilde{v}), \quad \tilde{v} \in V_k, \\ \sum_{k=1}^n C_k(q)v_k = 0, \end{cases}$$

where  $C_k(q)v_k = C(q)(0, \dots, 0, v_k, 0, \dots, 0)$ .

Unfortunately, the constraints  $C(q)$  that correspond to our identity or contact constraints are, in general, not surjective. Indeed, that would imply that the mapping  $v \mapsto v \circ q$  from  $V$  to  $\mathcal{C}^p(M, \mathbb{R}^d)$  is surjective, which would make the Banach norm on  $\mathcal{C}^p(M, \mathbb{R}^d)$  equivalent to a Hilbert norm. Hence, the optimality condition of [2] cannot be applied in a fully general infinite-dimensional context. However, surjectivity becomes almost straightforward when these constraints are discretized to a finite number. They are true as soon as the points involved in the constraints are all distinct, which is a mild assumption. We now proceed to the description of a discrete version of this approach.

#### 4. DISCRETE APPROXIMATIONS

**4.1. The Discrete Framework.** As an example, and to simplify the presentation, we detail our implementation for multi-shape problems in which shapes interact (through constraints) with a background, but not directly with each other, just like in Figure 1. Direct interactions between shapes can be handled in a similar way.

We first apply this to identity constraints, which only require the shapes to be discretized into a sets of points. We will then discuss sliding constraints, which will require more structure in order to define normal frames to the boundary.

We consider  $n - 1$  objects, discretized into point sets, so that  $M_k$  is a finite set of  $l_k$  indices for each  $k$ , and  $q^{(k)} : M_k \rightarrow (\mathbb{R}^d)^{l_k}$ . Let  $x_j^{(k)} = q^{(k)}(j)$  and  $x^{(k)} = (x_1^{(k)}, \dots, x_{l_k}^{(k)})$ , for  $k = 1, \dots, n - 1$ . In the case of a triangulated surface,  $x^{(k)}$  is simply the collection of corresponding vertices. We add as  $n$ -th object the boundary of the background (i.e., the union of all the other objects), defined by  $M_n = (\{1\} \times M_1) \cup \dots \cup (\{n - 1\} \times M_{n-1})$ , and  $q^{(n)} : M_n \rightarrow (\mathbb{R}^d)^{l_1 + \dots + l_{n-1}}$ . We let  $z_j^{(k)} = q^{(n)}(k, j)$ ,  $z^{(k)} = (z_1^{(k)}, \dots, z_{l_k}^{(k)})$  and  $z = (z^{(1)}, \dots, z^{(n-1)})$  (a

collection of  $l_n = l_1 + \dots + l_{n-1}$  points). For triangulated surfaces, each  $z^{(k)}$  represents the collection of vertices of the  $k$ -th objects, seen from “outside”, from the background. In this configuration, we should have  $x^{(k)} = z^{(k)}$ .

Let  $V_1, \dots, V_n$  be Hilbert spaces of vector fields of class  $\mathcal{C}^p$ ,  $p \geq 1$ , with respective reproducing kernel  $K_{V_1}, \dots, K_{V_n}$ . Assume that end-point cost functions  $U_1(x^{(1)}), \dots, U_{n-1}(x^{(n-1)})$  are defined, typically measuring the discrepancy between each collection of points and an associated target. We assume similar functions  $\tilde{U}_1(z^{(1)}), \dots, \tilde{U}_{n-1}(z^{(n-1)})$  for the background, typically using  $U_j = \tilde{U}_j$ . Then, a control consists in  $v = (v_1, \dots, v_n) \in L^2(0, 1; V_1 \times \dots \times V_n)$ , and we want to minimize the cost functional

$$\frac{1}{2} \sum_{k=1}^n \int_0^1 \|v_k(t)\|_{V_k}^2 dt + \sum_{k=1}^{n-1} U_k(x^{(k)}(1)) + \sum_{k=1}^{n-1} \tilde{U}_k(z^{(k)}(1)),$$

with the deformation of each object given by

$$\begin{cases} \partial_t x_j^{(k)} = v_k(x_j^{(k)}) & j = 1, \dots, m_k, k = 1, \dots, n-1, \\ \partial_t z_j^{(k)} = v_n(z_j^{(k)}), & j = 1, \dots, m_k, k = 1, \dots, n-1, \end{cases}$$

almost everywhere on  $[0, 1]$ .

*Reduction to a finite dimensional control space.* For  $y$  and  $y'$  ordered families of points in  $\mathbb{R}^d$ , let  $K^{(k)}(y, y')$  be the matrix formed with all  $d \times d$  blocks  $K_{V_k}(y_i, y'_j)$ , and let  $K^{(k)}(y) = K^{(k)}(y, y)$ , for  $k = 1, \dots, n$ . Since the problems only depend on the values taken by  $v_1, \dots, v_n$  on their corresponding point-set trajectories  $x^{(1)}, \dots, x^{(n-1)}, z$ , the optimal vector fields take the form

$$\begin{aligned} v_k(\cdot) &= K^{(k)}(\cdot, x^{(k)})\alpha^{(k)}, \quad k = 1, \dots, n-1, \\ v_n(\cdot) &= K^{(n)}(\cdot, z)\beta, \end{aligned}$$

for some families of  $d$ -dimensional vectors  $\alpha^{(1)}, \dots, \alpha^{(n-1)}, \beta$ . The problem can therefore be reduced to the finite-dimensional optimal control problem consisting in minimizing the cost functional

$$\begin{aligned} E(\alpha, \beta, x, z) &= \frac{1}{2} \sum_{k=1}^{n-1} \int_0^1 \alpha^{(k)} \cdot (K^{(k)}(x^{(k)})\alpha^{(k)}) dt + \frac{1}{2} \int_0^1 \beta \cdot (K^{(n)}(z)\beta) dt \\ &\quad + \sum_{k=1}^{n-1} U_k(x^{(k)}(1)) + \sum_{k=1}^{n-1} \tilde{U}_k(z^{(k)}(1)) \end{aligned}$$

subject to (almost everywhere along  $[0, 1]$ )

$$\begin{cases} \partial_t x^{(k)} = K^{(k)}(x^{(k)})\alpha^{(k)}, \\ \partial_t z = K^{(n)}(z)\beta, \end{cases}$$

in addition to identity or sliding constraints described below.

**4.2. Identity Constraints.** For identity constraints, the associated constrained optimal control problem consists in minimizing the cost functional  $E(\alpha, \beta, x, z)$  above, subject to the identity constraints

$$z^{(k)} = x^{(k)}, \quad k = 1, \dots, n-1,$$

everywhere along  $[0, 1]$ , which ensures that the objects and the background move concurrently.

Extending  $E$  with the augmented Lagrangian method, we introduce coefficients  $\lambda^{(k)}$ ,  $k = 1, \dots, n-1$  (where  $\lambda^{(k)}$  has the same dimension as  $x^{(k)}$ ) and  $\mu > 0$ , defining

$$\begin{aligned} E_{\lambda,\mu}(\alpha, \beta, x, z) = & \frac{1}{2} \sum_{k=1}^{n-1} \int_0^1 \alpha^{(k)} \cdot (K^{(k)}(x^{(k)})\alpha^{(k)}) dt + \frac{1}{2} \int_0^1 \beta \cdot (K^{(n)}(z)\beta) dt + \sum_{k=1}^{n-1} U_k(x^{(k)}(1)) \\ & + \sum_{k=1}^{n-1} \tilde{U}_k(z^{(k)}(1)) - \sum_{k=1}^{n-1} \int_0^1 \lambda^{(k)} \cdot (x^{(k)} - z^{(k)}) dt + \frac{\mu}{2} \sum_{k=1}^{n-1} \int_0^1 |x^{(k)} - z^{(k)}|^2 dt, \end{aligned}$$

which will be minimized subject almost everywhere along  $[0, 1]$ , with

$$\begin{cases} \partial_t x^{(k)} = K^{(k)}(x^{(k)})\alpha^{(k)}, \\ \partial_t z = K^{(n)}(z)\beta. \end{cases}$$

From the constraints,  $L_{\lambda,\mu}$  can be considered as a function of  $\alpha$  and  $\beta$  only. The computation of the gradient of  $L$  follows the general scheme described in Section 2.2 for the basic LDDMM algorithm. See Appendix C for detailed formulas and computations.

**4.3. Sliding Interface.** Assume that the parameter sets  $M_k$  are vertices of pure oriented, simplicial complexes  $T_k$  of dimension  $r_k < d$  (we will however only provide implementation details for codimension  $d - r_k = 1$ ). We let  $F_k$  denote the set of facets of the  $k$ -th complex. We also assume that  $T_1, \dots, T_{n-1}$  are disjoint and that  $T_n$  is their union,  $T_n = \bigcup_{k=1}^{n-1} T_k$ . We also let  $F_n = \bigcup_{k=1}^{n-1} F_k$  (disjoint union).

The associated shape space is formed by functions  $q_k : M_k \rightarrow \mathbb{R}^d$  such that  $q_k(f)$  is not degenerate (i.e., has maximal dimension) for all  $f \in F_k$ . Each object is allowed to slide against the background. We will write  $x^{(k)} = q^{(k)}(M_k)$ ,  $k = 1, \dots, n-1$ , and  $z^{(k)} = q^{(n)}(M_k)$ ,  $z = (z^{(1)}, \dots, z^{(n-1)})$ , in accordance with our previous notation. If  $f \in F_k$  is a facet in  $T_k \subset T_n$ , we discretize (7) into

$$(12) \quad N^{(n)}(f) \cdot \left( \sum_{j \in f} (v_k(z_j^{(k)}) - v_n(z_j^{(k)})) \right) = 0,$$

where  $N^{(n)}(f)$  is a  $d \times (d - r_k)$  matrix spanning the normal space to  $q^{(n)}(f)$ , assumed to be defined as a smooth function of  $q^{(n)}$ . If  $r_k = d - 1$ , this is always possible, since  $N^{(n)}$  is a vector that can be taken as the cross product of  $z_{f,2} - z_{f,1}, \dots, z_{f,d} - z_{f,1}$  where  $z_{f,1}, \dots, z_{f,d}$  is any labeling of the vertices of  $q^{(n)}(f)$  ordered consistently with the orientation.

We now restrict to this case, with  $d = 3$ , so that shapes are triangulated surfaces in  $\mathbb{R}^3$ , as discussed in Section 2.2. For  $f \in F_k$  and  $j \in f$ , we denote by  $e_{j,f}$  the edge  $(z_{j''}^{(k)} - z_{j'}^{(k)})$  where  $j'$  and  $j''$  are the other two vertices of  $f$  such that  $(j, j', j'')$  is positively oriented. Similarly, let  $e'_{j,f} = (z_{j'}^{(k)} - z_j^{(k)})$  and  $e''_{j,f} = (z_{j''}^{(k)} - z_j^{(k)})$  be the two edges stemming from  $z_j^{(k)}$  so that

$$e'_{j,f} \times e''_{j,f} = 2 \text{area}(q^{(n)}(f)) \tilde{N}^{(n)}(f) =: 2N^{(n)}(f)$$

is the twice the area-weighted positively oriented normal  $N^{(n)}(f)$  to  $f$  in  $q^{(n)}(M_k)$ . Note that  $e_{j,f} = e''_{j,f} - e'_{j,f}$ .

With this notation, we can rewrite the constraint in the form

$$\sum_{j \in f} \det(e'_{j,f}, e''_{j,f}, v_k(z_j^{(k)}) - v_n(z_j^{(k)})) = 0.$$

holding for all  $f \in F_k$  and  $k = 1, \dots, n-1$ .

Introducing a Lagrange multiplier  $\lambda_f$  for each of these constraints, after reduction of the vector fields, which proceeds similarly to the identity constraints case, the augmented Lagrangian takes the form

$$(13) \quad E'_{\lambda, \mu}(\alpha, \beta, x, z) = \frac{1}{2} \sum_{k=1}^{n-1} \int_0^1 \alpha^{(k)} \cdot (K^{(k)}(x^{(k)})\alpha^{(k)}) dt + \frac{1}{2} \int_0^1 \beta \cdot (K^{(n)}(z)\beta) dt + \sum_{k=1}^{n-1} U_k(x^{(k)}(1)) \\ + \sum_{k=1}^{n-1} \tilde{U}_k(z^{(k)}(1)) - \sum_{k=1}^{n-1} \sum_{f \in F_k} \int_0^1 (\lambda_f \Gamma_f^{(k)}(x^{(k)}, z) - \frac{\mu}{2} \Gamma_f^{(k)}(x^{(k)}, z)^2) dt,$$

with

$$\Gamma_f^{(k)}(x^{(k)}, z) := \sum_{j \in f} \det \left( e'_{j,f}, e''_{j,f}, K^{(k)}(z_j^{(k)}, x^{(k)})\alpha^{(k)} - K^{(n)}(z_j^{(k)}, z)\beta \right).$$

Note that we reduced  $v_k$  to  $\sum_i K^{(k)}(x^{(k)})\alpha^{(k)}$  for  $k = 1, \dots, n-1$  and  $v_n$  to  $\sum_i K^{(n)}(z)\beta$ . The computation of the gradient of  $L$  is then straightforward, see the appendix for detailed formulas.

## 5. EXISTENCE AND CONVERGENCE RESULTS

A question naturally arising is whether our discrete approximation using triangulations converges to the continuous case as triangles get smaller and smaller. More precisely, assume that some  $n-1$  smooth initial surfaces  $S_{init}^k = q_{init}^{(k)}(M_k)$  are triangulated, with increasingly fine triangulations  $q_{init}^{(k,\ell)} : M_{k,\ell} \rightarrow \mathbb{R}^3$ ,  $\ell = 1, 2, \dots$ , where  $M_{k,\ell}$  labels the vertices of a simplicial complex  $T_{k,\ell}$  whose set of faces are  $F_{k,\ell}$ . The corresponding vertices  $x_{j,init}^{(k,\ell)}$ , background vertexes  $z_{j,init}^{(k,\ell)}$ , the area-weighted normals  $N^{(n,\ell)}(f)$  and the background faces  $F_{n,\ell}$  are defined for each  $\ell$  as in Section 4.3.

For each step  $\ell$ , we consider data attachment terms  $U_{k,\ell}$  and  $\tilde{U}_{k,\ell}$  for the corresponding triangulations, and we also let  $U_k$  and  $\tilde{U}_k$  be data attachment terms for the continuous problem. We denote by  $E_\ell$  and  $E$  the corresponding cost functions. In this section, we discuss whether a weak limit point  $(v_k, k = 1, \dots, n)$  of minimizers  $(v_{k,\ell}, k = 1, \dots, n)$  of the discrete problems is a minimizer of the limit problem as the triangulations become increasingly fine, and if such a limit point exists.

To ensure the existence and minimality of  $(v_k, k = 1, \dots, n)$ , we will need the following hypotheses on the triangulations:

(i) Vertices of the triangulations of each  $S_{init}^k$  belong to  $S_{init}^k$ :  $q^{(k,\ell)}(j) \in S_{init}^k$  for  $j = 1, \dots, l_k$  and  $k = 1, \dots, n-1$ .

(ii) The triangulations are nested: for any  $k = 1, \dots, n-1$  and integer  $\ell$ ,

$$\{x_{j,init}^{(k,\ell)}, j \in M_{k,\ell}\} \subset \{x_{j,init}^{(k,\ell+1)}, j \in M_{k,\ell+1}\}.$$

(iii) The maximum edge length in each sequence of triangulations goes to 0.

(iv) If  $\eta(k, \ell, f)$  is the length of the largest edge of a face  $f$ , and  $a(k, \ell, f)$  its area, the ratio

$$\frac{a(k, \ell, f)}{\eta(k, \ell, f)^2},$$

$f \in F_{n,\ell}$  is bounded away from 0 (uniformly in  $\ell$ ).

These assumptions ensure the following property.

(v) For each  $k = 1, \dots, n-1$ ,

$$\max_{f \in F_{k,\ell}, x \in \tau_f^k} \left| \frac{N^{(n,\ell)}(f)}{|N^{(n,\ell)}(f)|} - N_k(x) \right| \rightarrow 0$$

when  $\ell$  goes to infinity, where  $\tau_f^k$  is the geodesic triangle on  $S_{init}^k$  corresponding to  $f$ .

In other words, the discrete normals converge to the normal vector field on each surface.

We say that a sequence of triangulations that satisfies hypotheses (i)-(iv) *converges nicely* to the surfaces  $S_{init}^k$ ,  $k = 1, \dots, n$ . Note that if a sequence of triangulations  $(q^{(\ell)})$  converges nicely to a surface  $S$ , then for any diffeomorphism  $\varphi$ ,  $(\varphi \circ q^{(\ell)})$  converges nicely to  $\varphi(S)$ . For the rest of this section, we will assume that we are working with one such sequence. In this case, we easily get that, if the data attachment terms are the current norms described Appendix A, then  $\tilde{U}_{k,\ell}(x_{init}^{(k,\ell)})$  goes to  $U_k(q_{init}^k)$  (see Appendix A.3 for a proof). In particular, the sequence of minimizers  $(v_{k,\ell}, k = 1, \dots, n)_{\ell \in \mathbb{N}}$  is bounded in  $L^2(0, 1; V_1 \times \dots \times V_n)$  by

$$\max_{\ell \in \mathbb{N}} \left\{ \sum_{k=1}^{n-1} U_{k,\ell}(x_{init}^{(k,\ell)}) + \sum_{k=1}^{n-1} \tilde{U}_{k,\ell}(z_{init}^{(k,\ell)}) \right\} < \infty.$$

Consequently, this sequence does admit a weak limit point  $(v_k, k = 1, \dots, n)$ .

**5.1. Identity Constraints.** The case of identity constraints is easy, and comes from [2, Proposition 5]. More precisely, assume that

- (1) each  $V_k$  has continuous inclusion into  $\mathcal{C}_0^1(\mathbb{R}^3, \mathbb{R}^3)$
- (2) the sequences of triangulations converge nicely to the surfaces,
- (3) the data attachment terms  $U_{k,\ell}$  and  $U_k$  come from a current norm (see Appendix A.1) that only depends on  $k$ , with targets either fixed surfaces  $S_{target}^k$  or sequences  $q_{target}^{(k,\ell)}$  of triangulations that converge nicely to the target surfaces  $S_{target}^k$ .

Then any weak limit point of the sequence of minimizers  $(v_{k,\ell}, k = 1, \dots, n)_{\ell \in \mathbb{N}}$  is a minimizer for the continuous problem with identity constraints.

**5.2. Sliding Constraints.** For sliding constraints, one cannot directly apply [2, Proposition 5], because the constraints are not nested, even when the triangulations are. To obtain a consistent approximation, we need to relax the discrete problems. More precisely, assume that

- (1) each  $V_k$  has continuous inclusion into  $\mathcal{C}_0^2(\mathbb{R}^3, \mathbb{R}^3)$
- (2) the sequences of triangulations converge nicely to the surfaces,
- (3) the data attachment terms  $U_{k,\ell}$  and  $U_k$  come from a current norm (see Appendix A.1) that only depends on  $k$ , with targets either fixed surfaces  $S_{target}^k$  or sequences  $q_{target}^{(k,\ell)}$  of triangulations that converge nicely to the target surfaces  $S_{target}^k$ .

Then, there exists a sequence of positive numbers  $\varepsilon_\ell$ ,  $\ell \in \mathbb{N}$  going to zero at infinity such that any weak limit point of a sequence  $(v_{k,\ell}, k = 1, \dots, n)_{\ell \in \mathbb{N}}$  of minimizers of the discrete problem at step  $\ell$  *under the relaxed constraints*

$$\left| N^{(n,\ell)}(f) \cdot \left( \sum_{j \in f} (v_{k,\ell}(z_j^{(k,\ell)}) - v_{n,\ell}(z_j^{(k,\ell)})) \right) \right| \leq \varepsilon_\ell |N^{(n,\ell)}(f)|, \quad f \in F_{k,\ell}$$

is a minimizer for the continuous problem with sliding constraints. This is proved in the appendix. It should be noted that such sequences  $(v_{k,\ell})_{\ell \in \mathbb{N}}$  always exist. Indeed, by introducing controls  $\alpha^{(k,\ell)}$  and  $\beta^{(\ell)}$  such that  $v_{k,\ell} = K^{(k,\ell)}(\cdot, x^{(k,\ell)})\alpha^{(k,\ell)}$  for each  $k = 1, \dots, n-1$ , and  $v_{n,\ell} = K^{(n,\ell)}(\cdot, z^{(\ell)})\beta^{(\ell)}$ , we get an equivalent finite dimensional optimal control problem with smooth inequality constraints. Such problems are known to admit minimizers (see, for example, [60]).

The sliding problem with relaxed constraints can then be solved using an augmented Lagrangian method.

## 6. EXPERIMENTAL RESULTS

**6.1. Synthetic Example.** The first example is described in Figure 2. In this synthetic example, the template has two identical balls initially close to each other. In the target, the first ball (referred to as “Ball A”) gets bigger, and “impacts”

the other one (referred to as “Ball B”), which assumes an oblong, non-convex shape (the target shapes slightly overlap, so that an exact homeomorphic match cannot be achieved).

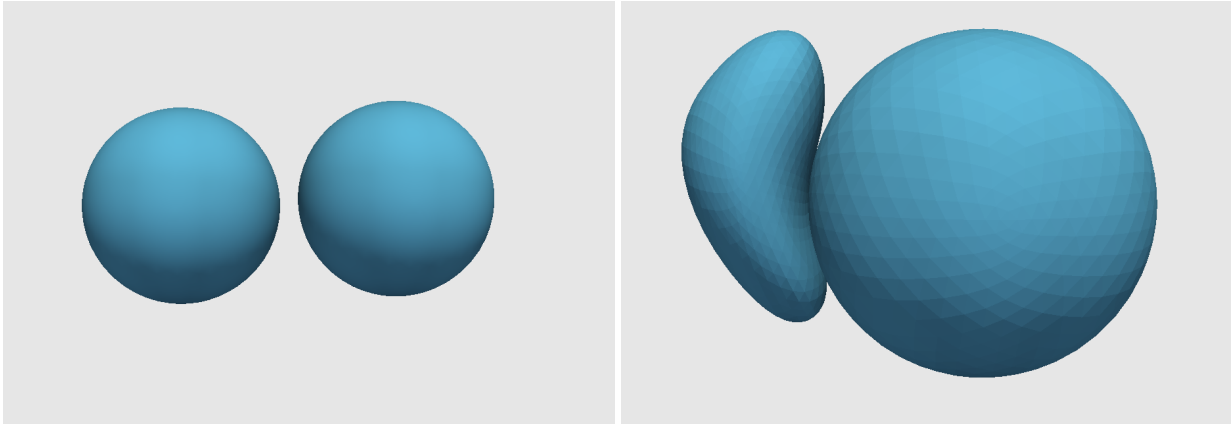


FIGURE 2. Template and target shapes for synthetic example

Our results, provided in Figures 3 to 6, illustrate our multishape deformation method, and use two complementary deformation indexes:

- (i) the tangent Jacobian, which is the Jacobian determinant of the surface-to-surface transformations, and which measures the ratio between the areas of elementary surface patches at each point before and after deformation;
- (ii) the normal Jacobian, which is the ratio of the Jacobian determinant (of the 3D diffeomorphism) to the tangent Jacobian, and which measures the ratio between the length of an infinitesimal line element normal to the surface after and before transformation.

These indexes are mapped on the deformed template image, which is close to the target.

Figure 3 compares the normal Jacobian of the shape and background deformations when using identity constraints. While shape diffeomorphisms characterize each shape transformation (uniform variation for Ball A, expansion at the top and compression otherwise for Ball B), the effect of compressing the space is clearly visible in the background deformation, when the two shapes get close to each other.

Figure 4 provides the corresponding tangent Jacobian, which is identical for shape and background transformation since we are using identity constraints.

Figures 5 and 6 compare the normal and tangent Jacobians for the synthetic experiment with sliding constraints. Regarding the former, the most notable difference is with Ball B, which shows an expansion pattern at the tips in its shape diffeomorphism which is inverse of the one observed with identity constraints. One plausible explanation is that sliding constraints allow the two shapes to use translation-like motion to position themselves differently, without the need for limiting the amount of shear in the background that would have resulted from identity constraints. The second notable difference can be noted in the background diffeomorphism, in which compression is mostly observed with Ball B. In contrast with the identity constraints, the tangent Jacobians are very different between shape and background diffeomorphisms. Note that Figure 6 uses two different color scales for the left and right panels because of the strong difference between the ranges of the Jacobians in each case. The background deformation, in particular, has a huge tangent expansion around the impact location, which cannot be observed in the shape deformations. Note that both patterns in the sliding case are very different from the one that was observed in the identity case.

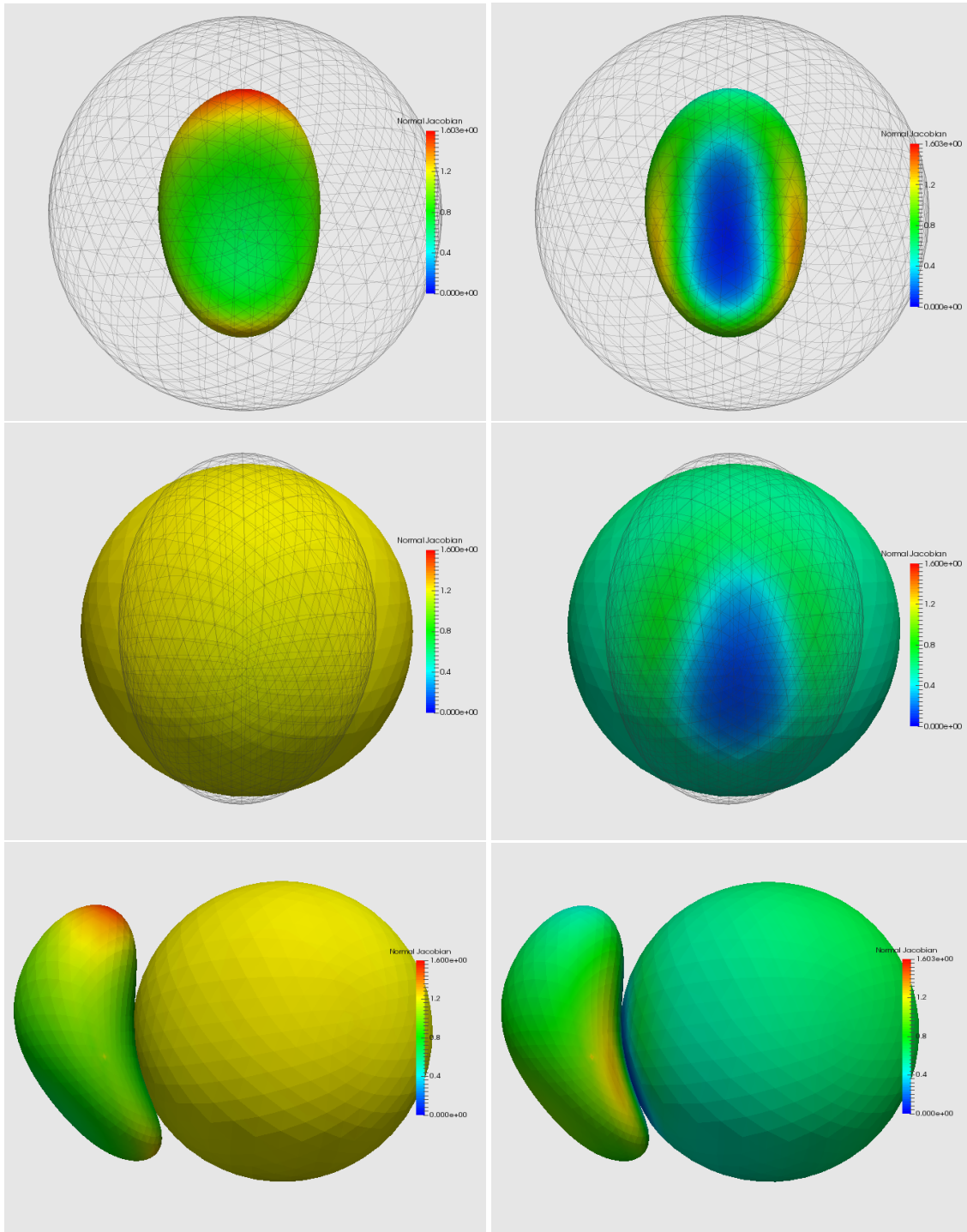


FIGURE 3. Three views of the normal Jacobian with identity constraints: shape diffeomorphisms (left) and background diffeomorphism (right).

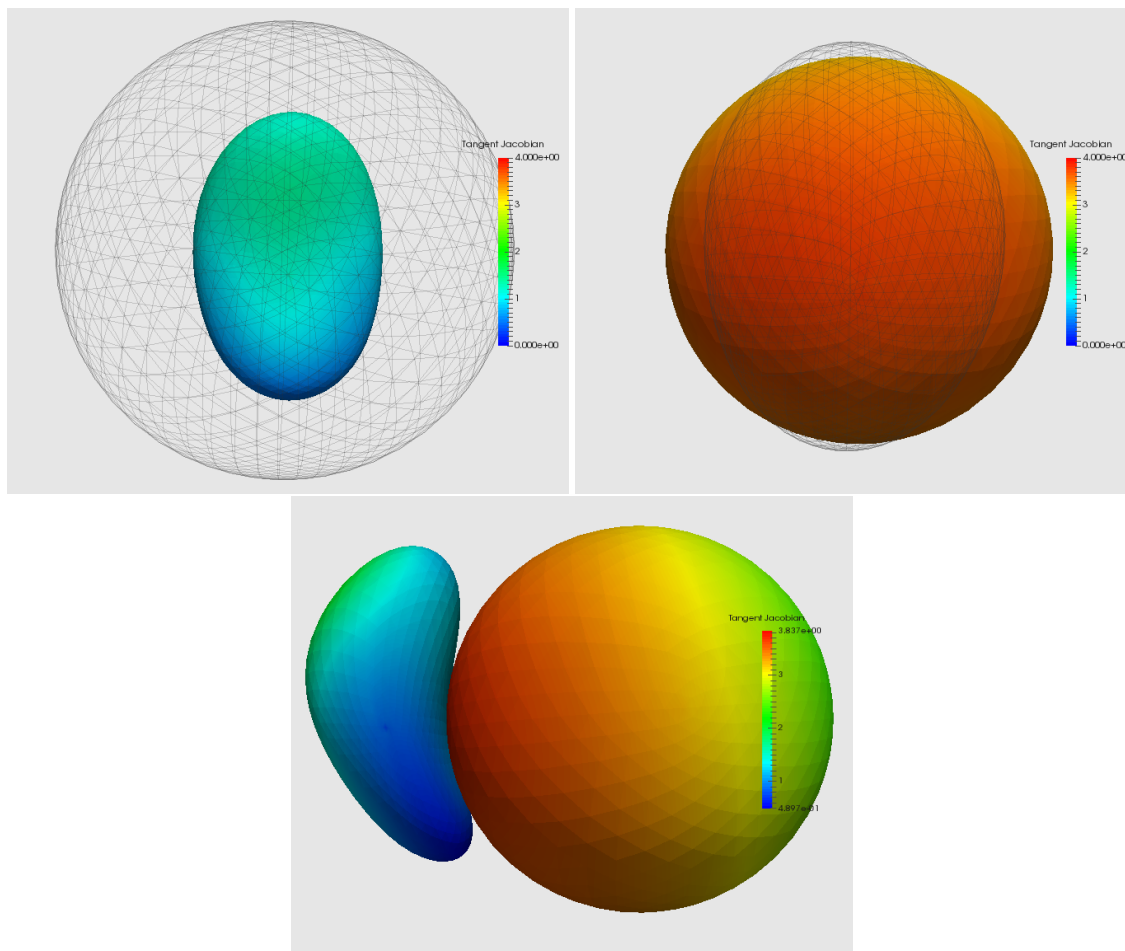


FIGURE 4. Tangential Jacobian: shape and background diffeomorphisms (identity constraints).

For comparison purposes, Figure 7 provides the result of the LDDMM algorithm using a single diffeomorphism. One observes a very strong compression effect for the normal jacobian resulting in an expansion observed on the tangent jacobian on Ball B, that was not observed in any of the constrained examples. The nice uniform expansion in Ball A that could be observed in the sliding constraint case is not observed either.

**6.2. Subcortical Structures.** We now describe an example mapping a group of three subcortical structures: hippocampus, amygdala and entorhinal cortex (ERC). The template and target sets are represented in Figure 8. One can observe shape changes in each structure, combined with a significant displacement of the ERC relative to the other two structures when comparing template to target. Because the structures were segmented independently, there is some overlap between the target hippocampus and amygdala.

Figures 9 and 10 provide the normal and tangent Jacobian obtained with identity constraints, while Figures 11 and 12 provide this information for sliding constraints. The two types of constraints provide similar deformation

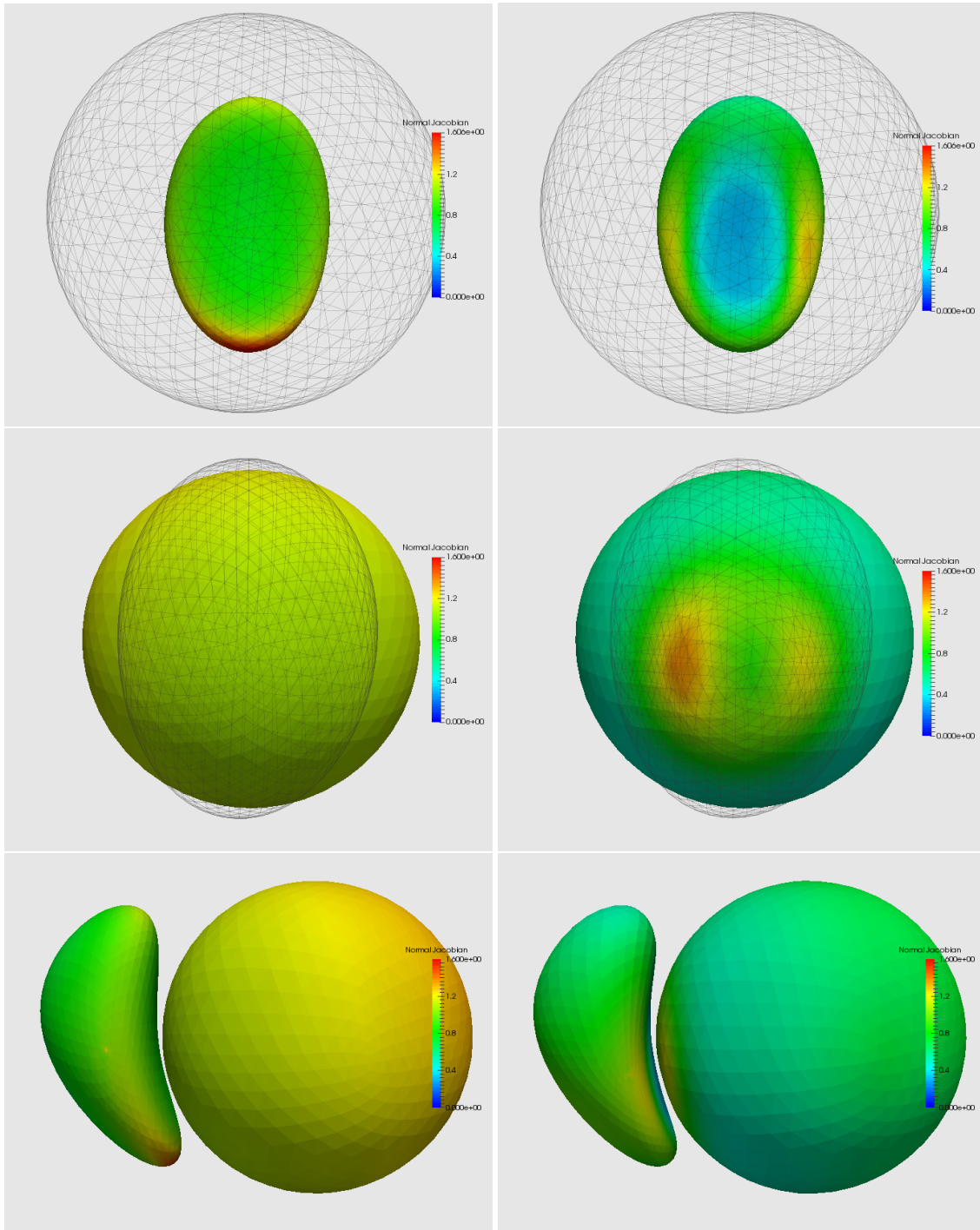


FIGURE 5. Three views of the normal Jacobian with sliding constraints: shape diffeomorphisms (left) and background diffeomorphism (right).

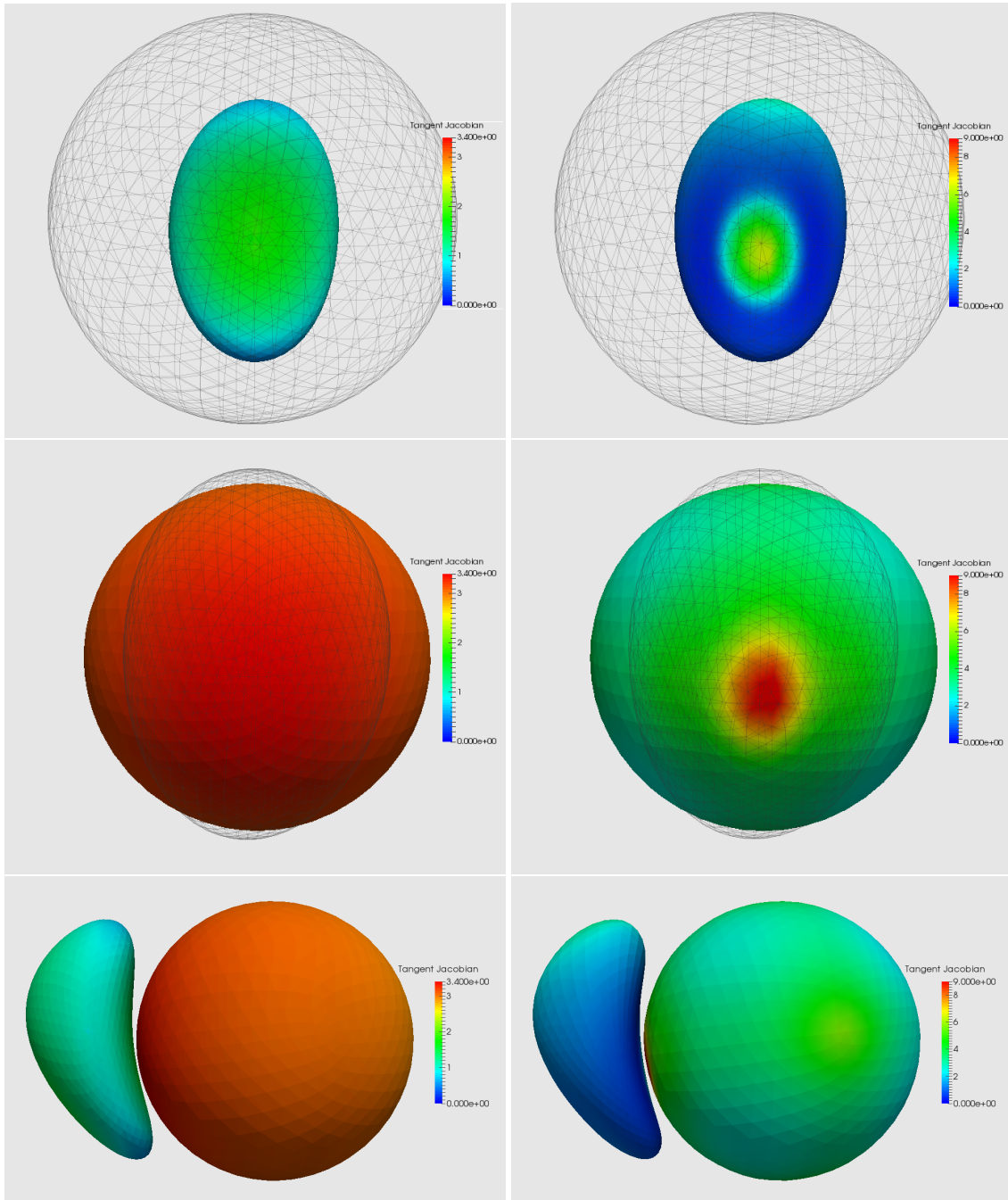


FIGURE 6. Three views of the tangent Jacobian with sliding constraints: shape diffeomorphisms (left) and background diffeomorphism (right).

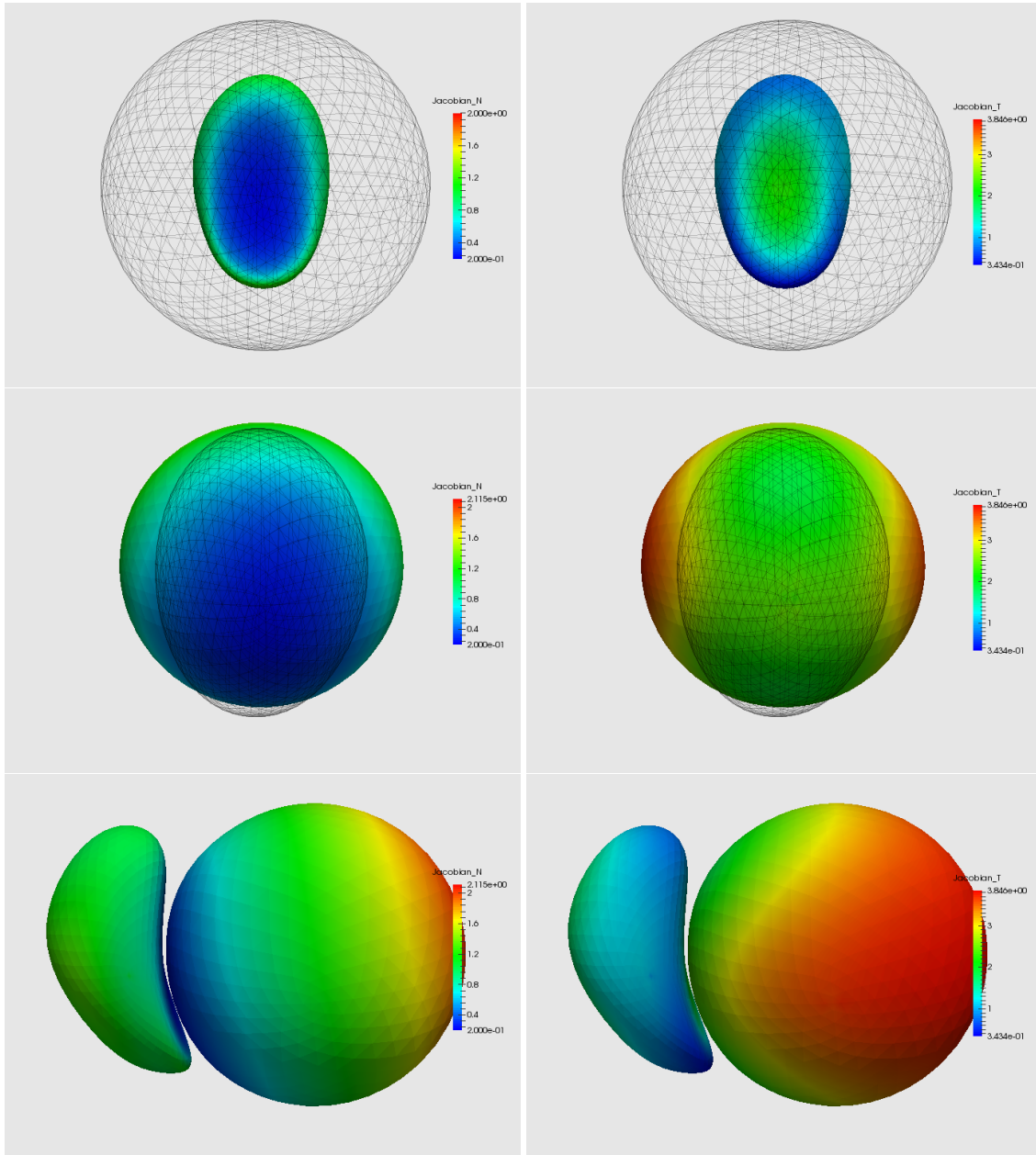


FIGURE 7. Three views of the Normal (left) and tangential Jacobians (right) when using a single diffeomorphism.

indices, especially for the normal jacobians (Figures 9 and 11). Minor differences in the tangent jacobian can be

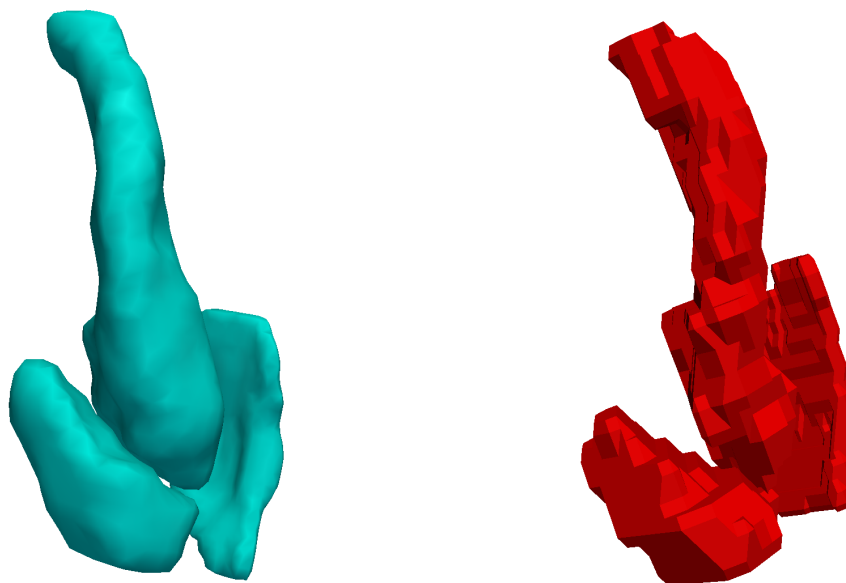


FIGURE 8. Template (blue) and target (red) shapes for subcortical structures. The hippocampus is the central shape, with the amygdala on its left and the ERC on its right.

observed (Figures 10 and 12). The deformation patterns associated to using a single diffeomorphism (Figure 13) are significantly different, though, exhibiting very strong compression, for example, where shapes are close to each other.

## 7. DISCUSSION

The previous approach provides a solution, using constrained optimal control, of the important issue of dealing with multiple objects with varying deformation properties for registration. We have focused on surface matching, numerically dealing with constraints using an augmented Lagrangian method. Note that a similar approach was introduced for plane curves in [2].

The formulation is quite general and can accommodate constraints in various forms, including the examples discussed in Section 3. The investigation of these additional applications will be the subject of future work. One of the limitations of the present implementation is the slow convergence of the augmented Lagrangian procedure, for which each minimization step is, in addition, high dimensional and computationally demanding. One possible alternative can be based on solving the optimality conditions (11) (which hold in the discrete case) by means of a numerical shooting method. This approach has, however, its own numerical challenges, because solving (11) requires the determination of  $\lambda$  such that the last equation (constraint) is satisfied, and this leads to a possibly ill-posed problem for systems in large dimension (see [2] for additional details).

We have illustrated our examples using deformation markers derived from the jacobian determinant. These markers are routinely used in shape analysis studies and led to important conclusion in computational anatomy. When dealing with multiple shapes, however, figures 7 and 13 show that, when using the classical LDDMM method with multiple shapes, these markers becomes as much, if not more, influenced by interactions between the shapes as by the changes in the shapes themselves. For this reason, multi-shape computational anatomy studies have applied registration methods separately to each shape, without ensuring that the obtained diffeomorphisms are consistent with each other. This

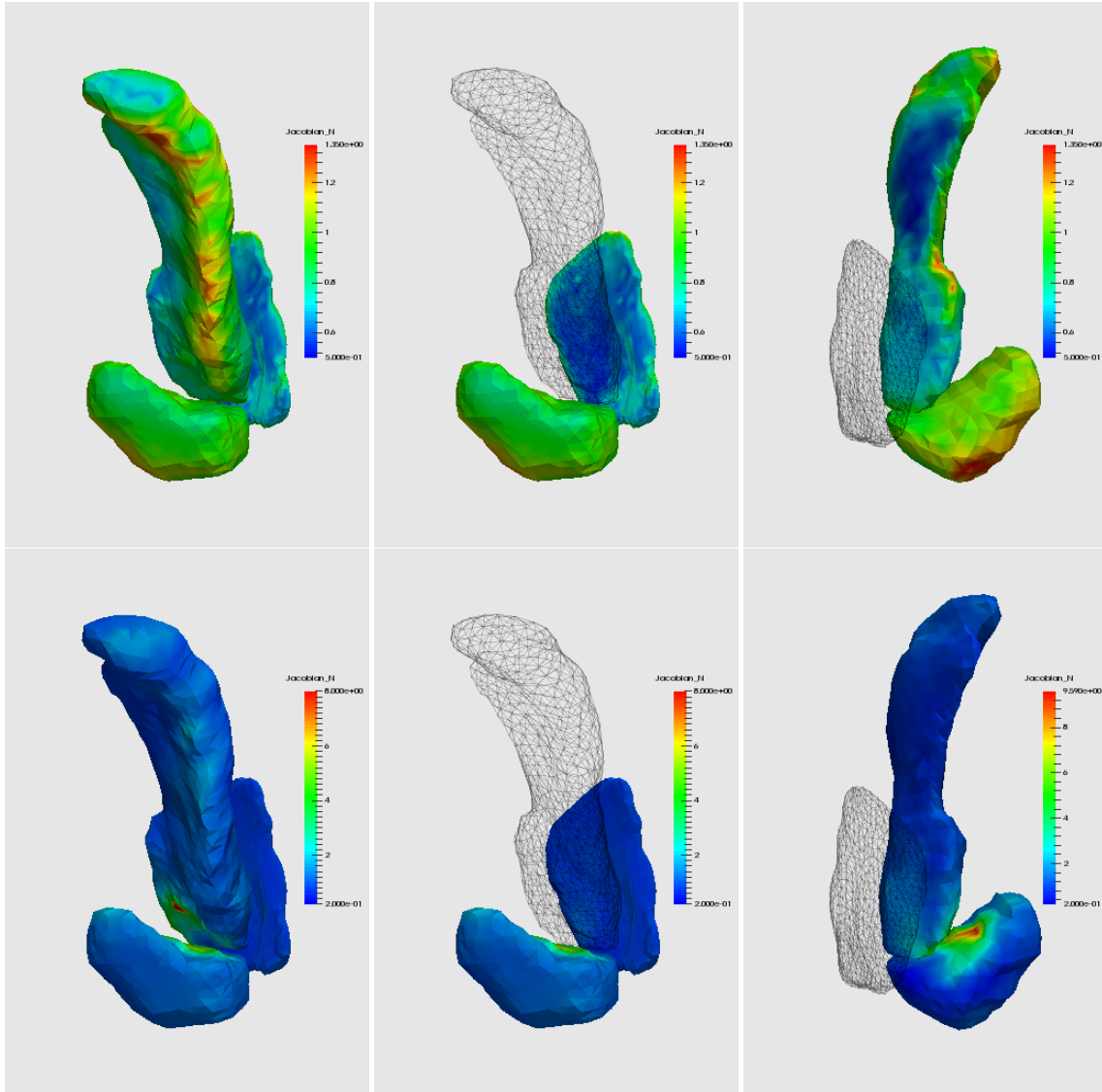


FIGURE 9. Three views of the normal Jacobian with identity constraints: First Row: Shape diffeomorphisms; Second Row: Background diffeomorphism.

limitation is addressed in the present paper, in which we exhibit deformation markers that are meaningful in describing tangential and normal surface stretching, while being consistently associated to a global transformation of the space.

The method presented in this paper does not directly address the important problem of contact between two objects, where two independent shapes collide and slide along each other, possibly separating again afterwards. Rather, it sidesteps it by enforcing a diffeomorphic transformation of the background during the deformation, still allowing it to undergo larger deformations by choosing an appropriate kernel. Consequently, if the two objects start away from one another, they interact very little, but, as they get closer and closer to one another they repel each other slightly so that

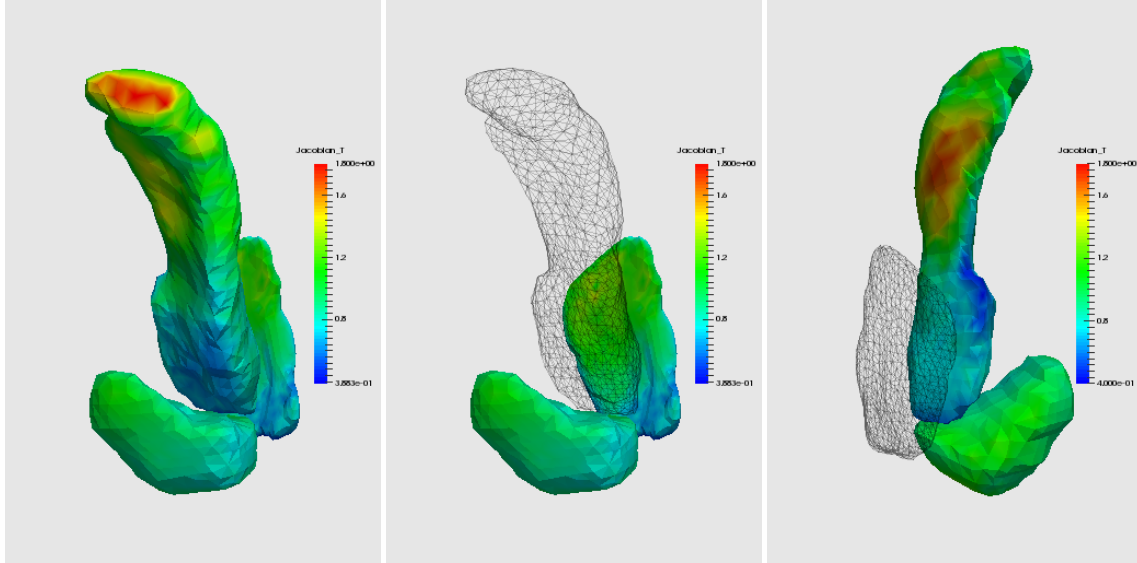


FIGURE 10. Three views of the tangent Jacobian with identity constraints: Shape and background diffeomorphisms.

they never cross path. This lets us enjoy the positive aspects of the LDDMM methods, such as the regularity of the transformations, so that fine enough triangulations do not degenerate along the deformation.

Now, in the continuous case, as the scale of the background kernel goes to zero, the optimal deformations likely converge to the case where shapes can collide. However, in the case of a discrete triangulation, as the scale of the background kernel gets much smaller than the length of the edges of the triangles, the different shapes will stop interacting with one another, possibly passing through one another. Hence, to model collisions, an equilibrium must be found between the refinement of the discretization and the scale of the background kernel.

Our point of view was mainly focused on equality constraints, but we briefly mentioned inequality constraints in Section 5. While algorithms exist to numerically solve such problems, they present many difficulties from a mathematical viewpoint in the continuous (infinite dimensional) case. However, the ability to tackle such constraints would be of great interest, as they could possibly be used, for example, to actually solve the contact problem.

#### APPENDIX A. EXAMPLES OF DATA ATTACHMENT: CURRENT NORMS AND THEIR DERIVATIVES

Let us briefly describe the current norms and compute their derivative.

##### A.1. Current Norms for Submanifolds.

*Closed Surfaces.* If  $\mu$  is a scalar measure on  $\mathbb{R}^d$  and  $z$  a  $\mu$ -integrable  $\mathbb{R}^d$ -valued function defined on  $\text{support}(\mu)$ , we will denote by  $z\mu$  the vector measure such that

$$(z\mu | w) = \int_{\text{support}(\mu)} z \cdot w \, d\mu,$$

where  $z \cdot w$  denotes the standard euclidean dot product.

Vector measures of the form  $z\mu$  are continuous linear forms over any space that is continuously imbedded in  $C_0^0(\mathbb{R}^d, \mathbb{R}^d)$ , and in particular over any reproducing kernel Hilbert space  $W$ . For such a space, equipped with a reproducing kernel  $\chi$ , the operator norm of  $z\mu$  is given by

$$\|z\mu\|_\chi^2 = \iint z(x) \cdot (\chi(x, y)z(y)) \, d\mu(x) \, d\mu(y),$$

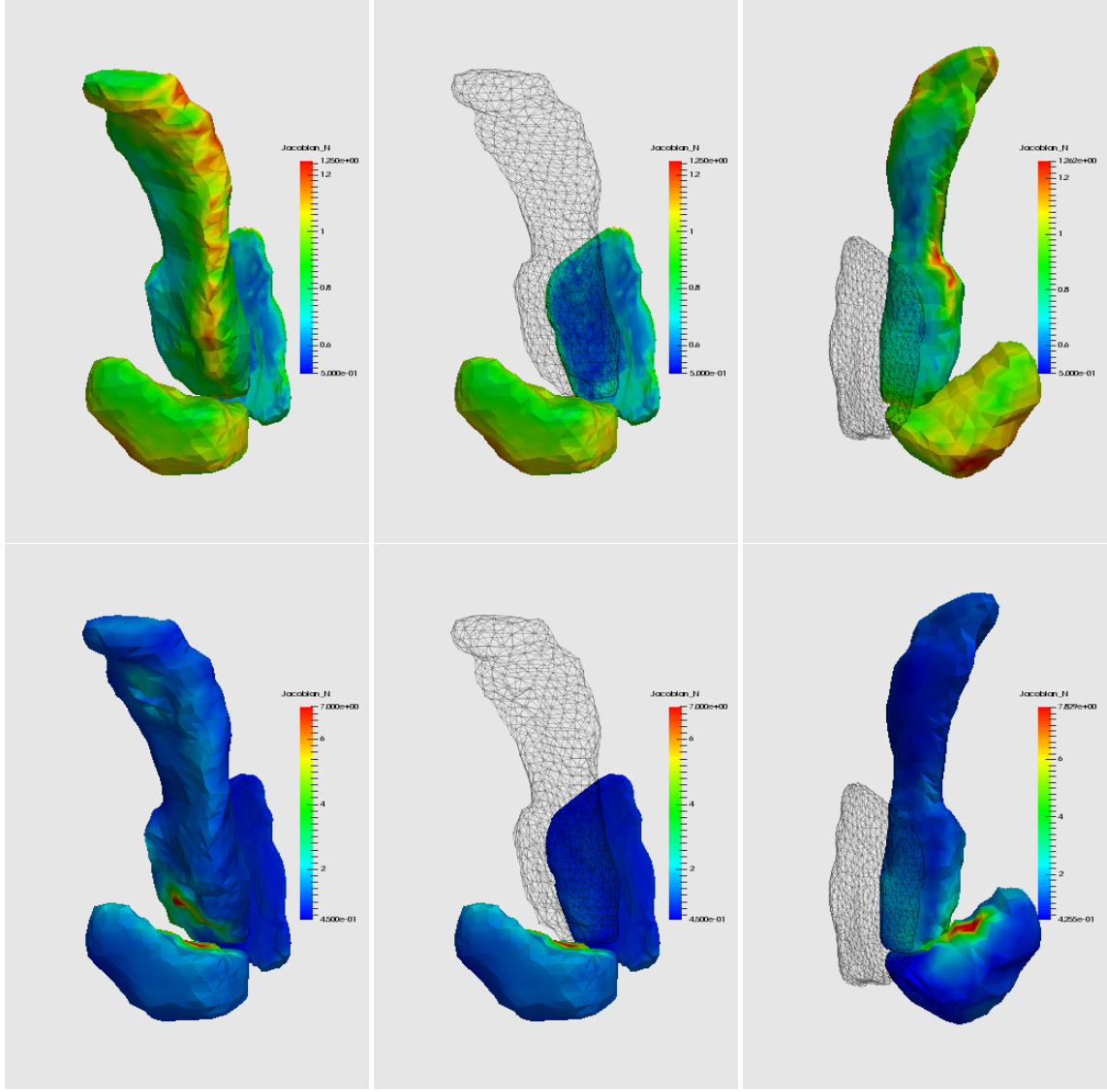


FIGURE 11. Three views of the normal Jacobian with sliding constraints: First Row: Shape diffeomorphisms; Second Row: Background diffeomorphism.

and more generally, the norm of the difference between two such measures is

$$\begin{aligned} \|z\mu - \tilde{z}\tilde{\mu}\|_{\chi}^2 &= \iint z(x) \cdot (\chi(x, y)z(y)) d\mu(x) d\mu(y) \\ &\quad - 2 \iint z(x) \cdot (\chi(x, y)\tilde{z}(y)) d\mu(x) d\tilde{\mu}(y) + \iint \tilde{z}(x) \cdot (\chi(x, y)\tilde{z}(y)) d\tilde{\mu}(x) d\tilde{\mu}(y). \end{aligned}$$

Note that  $W$  has no relationship with the reproducing kernel spaces used to induce deformations on the shapes we study all throughout the paper, except that both have a continuous inclusion in  $C_0^0(\mathbb{R}^d, \mathbb{R}^d)$ :  $\chi$  is different from  $K$ ,  $K_{V_1}$ , etc...

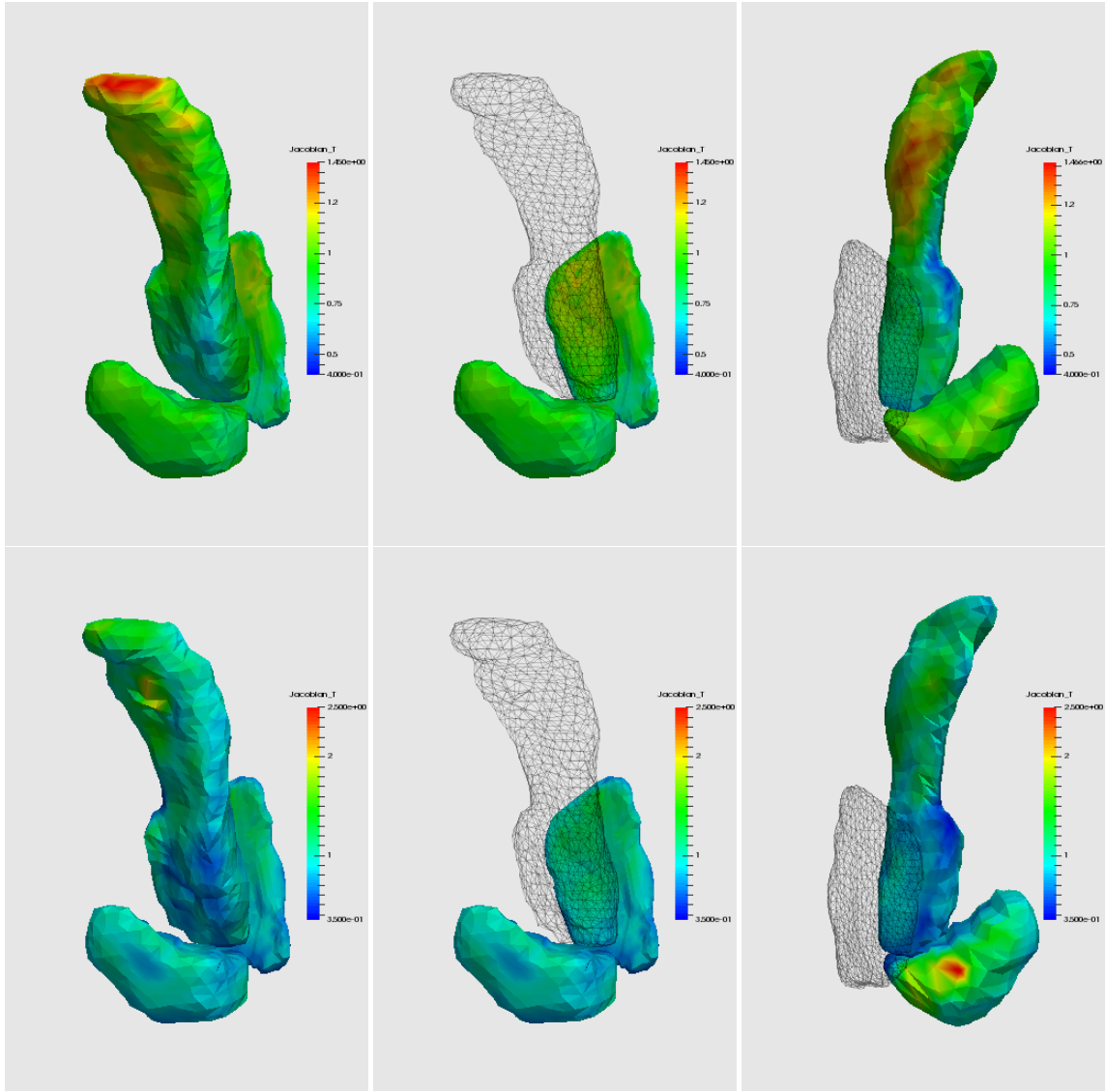


FIGURE 12. Three views of the tangent Jacobian with sliding constraints: First Row: Shape diffeomorphisms; Second Row: Background diffeomorphism.

One can deduce from this the surface-matching cost function introduced in [63], in which an oriented surface  $S$  is represented as a geometric current and a dual-RKHS norm between currents is used. Identifying surface currents with vector measures, this leads to the representation of  $S$  given by  $\mu_S = N_S \sigma_S$ , where  $N_S$  is the unit normal to  $S$  and  $\sigma_S$  its volume form. Assume that  $M$  (the parameter space) is an oriented 2D manifold so that  $S = q(M)$  is an embedding of  $M$  through  $q$ , and let  $\eta = q^* \mathcal{A}_S$  be the positively oriented volume form on  $M$  obtained by pulling back the area form  $\mathcal{A}_S$  of  $S$  by  $q$ . For  $m \in M$  let  $N_q(m) \in \mathbb{R}^3$  denote the “area-weighted normal” to  $S = q(M)$  at  $q(m)$ , defined

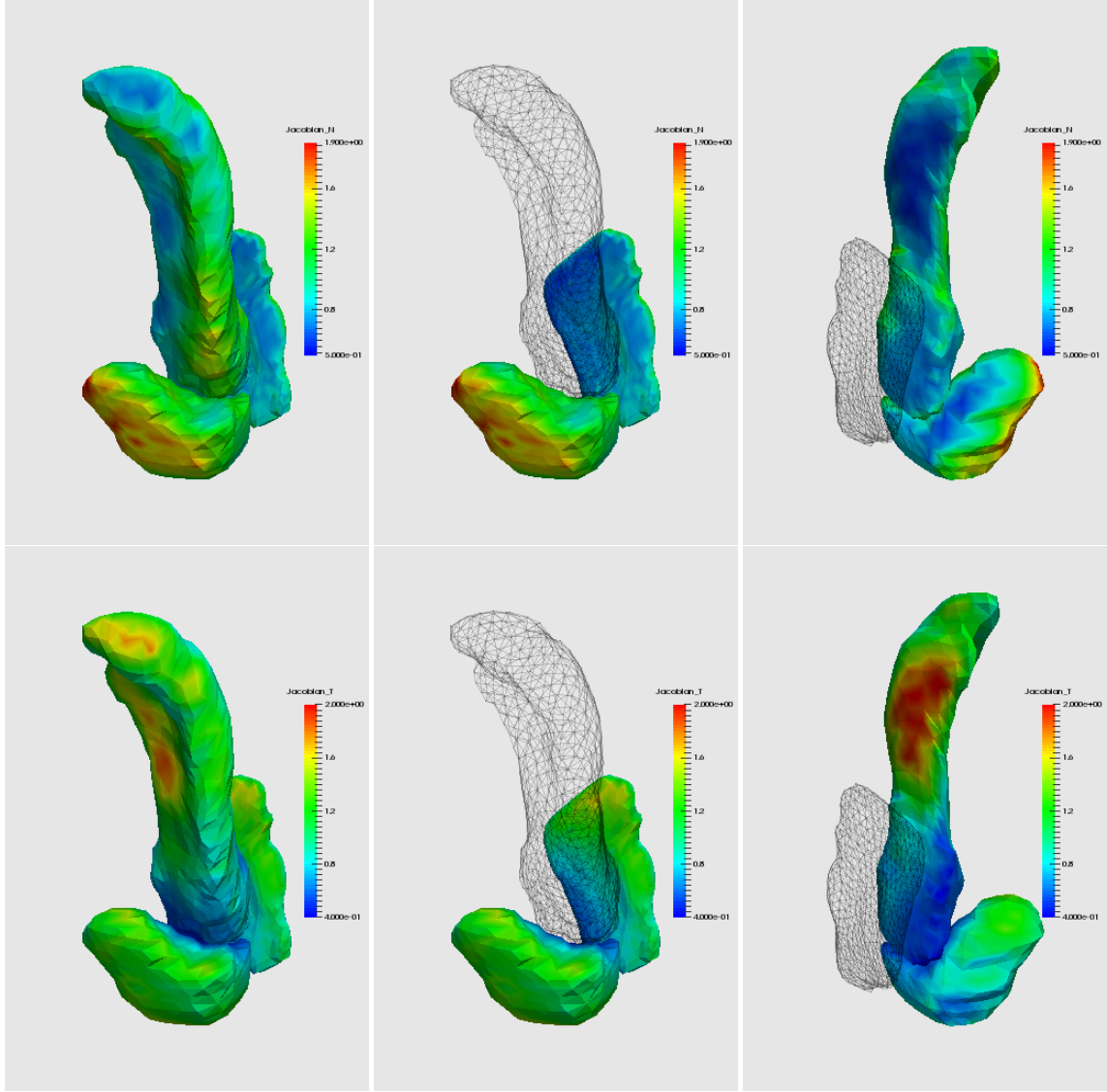


FIGURE 13. Three views of the normal (up) and tangent Jacobians (down) when using a single diffeomorphism.

by  $N_q(m) = dq_m e_1 \times dq_m e_2$  where  $(e_1, e_2)$  is an arbitrary basis of  $T_m M$  such that  $\eta_x(e_1, e_2) = 1$ . Then

$$(\mu_S | w) = \int_M (w \circ q \cdot N_q) d\eta,$$

for every  $w \in C_0^0(\mathbb{R}^3, \mathbb{R}^3)$ . Note that, for  $x = q(m) \in S$ , if we denote  $N_S(x) = \frac{N_q(m)}{|N_q(m)|}$  the unit normal to  $S$  at  $x$ , we obtain

$$(\mu_S | w) = \int_S (w \cdot N_S) d\mathcal{A}_S.$$



FIGURE 14. Midpoint of the optimal deformation with multishape identity constraints (left), multishape sliding constraints (center) and single diffeomorphism (right).

Now, given a reproducing kernel  $\chi$  and a target surface  $\tilde{S} = \tilde{q}(M)$ , we define the surface-matching cost by

$$\begin{aligned}
 (14) \quad U(q) = \|\mu_{q(M)} - \mu_{\tilde{q}(M)}\|_{\chi}^2 = & \iint_{S \times S} N_S(x) \cdot (\chi(x, y) N_S(y)) d\mathcal{A}_S(x) d\mathcal{A}_S(y) \\
 & - 2 \iint_{S \times \tilde{S}} N_S(x) \cdot (\chi(x, y) N_{\tilde{S}}(y)) d\mathcal{A}_S(x) d\mathcal{A}_{\tilde{S}}(y) \\
 & + \iint_{\tilde{S} \times \tilde{S}} N_{\tilde{S}}(x) \cdot (\chi(x, y) N_{\tilde{S}}(y)) d\mathcal{A}_{\tilde{S}}(x) d\mathcal{A}_{\tilde{S}}(y)
 \end{aligned}$$

*General Submanifolds with Boundary.* The previous cost function is actually a special case of the more general framework in which one compares compact  $k$ -dimensional oriented submanifolds of  $\mathbb{R}^d$ , which we briefly discuss hereafter. Given such a manifold,  $S$ , with a global parametrisation  $q : M \rightarrow S$ , one can associate to any  $\omega \in C_0^p(\mathbb{R}^d, (\Lambda^k \mathbb{R}^d)^*)$  (the set of  $C^p$  differential  $k$ -forms on  $\mathbb{R}^d$  that vanish at infinity), its integral

$$(C_S | \omega) = \int_S \omega = \int_M q^* \omega,$$

where  $q^* \omega$  denotes the pull-back of  $\omega$  on  $M$ . An RKHS,  $\tilde{W}$ , of such forms, is a Hilbert space continuously embedded in  $C_0^p(\mathbb{R}^d, (\Lambda^k \mathbb{R}^d)^*)$ , with kernel  $\tilde{\chi}(x, y)$  taking values in the space of bilinear functions on  $\Lambda^k \mathbb{R}^d \times \Lambda^k \mathbb{R}^d$ . The linear form  $C_S$  then belongs in  $\tilde{W}^*$ , and is a special form of a *geometric current*, as defined in [20]. If  $S = q(M)$  and  $\tilde{S}$  is a target manifold, they can be compared using the operator norm

$$(15) \quad U(q) = \|C_{q(M)} - C_{\tilde{S}}\|_{\tilde{W}^*}^2.$$

Now to apply our minimization algorithm, we need to be able to compute the derivative of such a function.

*Derivative of Current Norms.* If we consider  $\hat{q} : \hat{M} \doteq (-1, 1) \times M \rightarrow \mathbb{R}^d$  a smooth perturbation of  $q$  such that  $q_\varepsilon = q + \varepsilon \delta q + o(\varepsilon)$  where  $q_\varepsilon(x) = \hat{q}(\varepsilon, x)$  for  $\varepsilon \in (-1, 1)$  and  $x \in M$ , we have, for  $M_\varepsilon \doteq \{\varepsilon\} \times M$ ,

$$(dU_q | \delta q) = \frac{d}{d\varepsilon} \left( \int_M q_\varepsilon^* \omega \right) \Big|_{\varepsilon=0} = \frac{d}{d\varepsilon} \left( \int_{M_\varepsilon} \hat{q}^* \omega \right) \Big|_{\varepsilon=0} = \int_{M_0} \mathcal{L}_{\partial/\partial\varepsilon}(\hat{q}^* \omega),$$

where  $\mathcal{L}_{\partial/\partial\varepsilon}$  is the Lie derivative along the vector field  $\frac{\partial}{\partial\varepsilon}$  on  $\hat{M}$  (which is equal to  $(1, 0) \in \mathbb{R} \times T_m M$  at any location  $(\varepsilon, x) \in \hat{M}$ ) and

$$(16) \quad \omega = 2K_{\tilde{W}}(C_{q(M)} - C_S),$$

with  $K_{\tilde{W}}$  the isometry from  $\tilde{W}^*$  to  $\tilde{W}$ . We next show that

$$(dU_q | \delta q) = \int_M \alpha_q \cdot \delta q \operatorname{vol}_M + \int_{\partial M} \beta_q \cdot \delta q \operatorname{vol}_{\partial M},$$

where  $\operatorname{vol}_M$  and  $\operatorname{vol}_{\partial M}$  are the positive Riemannian volume forms on  $M$  and  $\partial M$ , and  $\alpha_q : M \rightarrow \mathbb{R}^d$  (resp.  $\beta_q : \partial M \rightarrow \mathbb{R}^d$ ) is such that  $\alpha_q(x)$  is normal to  $S = q(M)$  (resp.  $\beta_q(x)$  is normal to  $\partial S = q(\partial M)$ ) at  $q(x)$ . Using the Cartan magic formula we get

$$\mathcal{L}_{\partial/\partial\varepsilon}(q^* \omega) = i_{\partial/\partial\varepsilon} d(q^* \omega) + d(i_{\partial/\partial\varepsilon}(q^* \omega)),$$

so that, applying the Stokes theorem,

$$(dU_q | \delta q) = \int_{M_0} i_{\partial/\partial\varepsilon}(\hat{q}^* d\omega) + \int_{\partial M_0} i_{\partial/\partial\varepsilon}(\hat{q}^* \omega),$$

where  $i_{\partial/\partial\varepsilon}$  denotes the contraction operator. Note that, for  $\xi_1, \dots, \xi_k \in T_x M$ ,

$$\begin{aligned} i_{\partial/\partial\varepsilon}(\hat{q}^* d\omega)_{(0,x)}(\xi_1, \dots, \xi_k) &= d\omega_{q(x)}(\delta q(x), dq_x \xi_1, \dots, dq_x \xi_k) \\ &= d\omega_{q(x)}(\delta q^\perp(x), dq_x \xi_1, \dots, dq_x \xi_k), \end{aligned}$$

where  $\delta q^\perp(x)$  denotes the projection of  $\delta q(x)$  on  $T_{q(x)} S^\perp$  (since the form vanishes if  $\delta q(x) \in T_{q(x)} S = T_{q(x)} q(M)$ ). Since the set of  $k$ -forms is a one-dimensional space on  $M$ , this means that we can write, for some function  $\alpha_q$  such that  $\alpha_q(x) \in (T_{q(x)} S)^\perp$ , with  $x \in M$ ,

$$i_{\partial/\partial\varepsilon}(q^* d\omega)_{(0,x)} = ((\delta q \cdot \alpha_q) \operatorname{vol}_M)_x.$$

Similarly,

$$i_{\partial/\partial\varepsilon}(q^* \omega_q)_{(0,x)} = ((\delta q \cdot \beta_q) \operatorname{vol}_{\partial M})_x,$$

for  $\beta_q(x) \in (T_{q(x)} \partial S)^\perp$ .

The data term defined in (15) is derived from this general construction, using the fact that two-forms in  $\mathbb{R}^3$  (or  $(d-1)$ -forms in  $\mathbb{R}^d$ ) can be identified with vector fields via  $\omega_x(e_1, e_2) = w(x) \cdot (e_1 \times e_2)$ . The current  $C_S$  is then identified with the vector measure  $\mu_S$ . The form  $\omega$  introduced in (16) becomes, introducing a global parametrization  $\tilde{q} : M \rightarrow \tilde{S}$  of the target  $\tilde{S}$ , the vector field

$$w(\cdot) = 2 \int_{\mathbb{R}^d} \chi(\cdot, y) d(\mu_{q(M)} - \mu_{\tilde{q}(M)})(y).$$

With this identification, we have  $\alpha_q = \operatorname{div}(w) \circ q N_q$  where  $N_q$  is the oriented ‘‘area-weighted’’ normal to  $S$  at  $q(x)$  defined previously, and  $\beta_q = \tau_q \times w \circ q$ , where  $\tau_q$  is the oriented ‘‘length-weighted’’ tangent to  $q(\partial M)$  given as  $\tau_q(x) = dq_x e_1$ , where  $e_1$  is the unit positively oriented tangent vector at  $x$  along  $\partial M$ .

**A.2. Current Norms for Triangulated Surfaces.** Returning to surfaces, the discrete case, in which triangulated surfaces are compared, is, for practical purposes, even more important. We here also consider the case  $M = \{1, \dots, m\}$ , with an additional family  $F$  of facets, which are ordered triples  $(i, j, k)$  with  $i, j, k \in M$ . (We assume that  $F$  is consistent with a manifold structure: The set  $V_i$  of indices that share a facet with  $i$  must form a chain and no pair of indices can be included in more than two facets.)

Given a one-to-one mapping  $q : M \rightarrow \mathbb{R}^3$ , define  $S_q$  as the collection of triangles  $S_q = \{(q(i), q(j), q(k)), (i, j, k) \in F\}$ . If  $f = (i, j, k)$ , let  $q(f) = (q(i), q(j), q(k))$ ,  $N_q(f) = \frac{1}{2}(q(j) - q(i)) \times (q(k) - q(i))$  and  $c_q(f) = (q(i) + q(j) + q(k))/3$  respectively denote the triangle, area-weighted normal and center associated to the facet  $f$ . Following [63], we define the vector measure associated to  $q$  by

$$\mu_q = \sum_{f \in F} N_q(f) \delta_{c_q(f)}.$$

Here,  $\delta_x$  (with  $x \in \mathbb{R}^3$ ) denotes the atomic measure of mass 1 with support  $\{x\}$ . The (discrete) surface matching cost associated to a target  $\tilde{q}$  with set of faces  $\tilde{F}$  is then defined by

$$(17) \quad \begin{aligned} U(q) = \|\mu_q - \mu_{\tilde{q}}\|_{\chi}^2 = & \sum_{f \in F} \sum_{f' \in F} N_q(f) \cdot (\chi(c_q(f), c_q(f')) N_q(f')) \\ & - 2 \sum_{f \in F} \sum_{\tilde{f} \in \tilde{F}} N_q(f) \cdot (\chi(c_q(f), c_{\tilde{q}}(\tilde{f})) N_{\tilde{q}}(\tilde{f})) \\ & + \sum_{\tilde{f} \in \tilde{F}} \sum_{\tilde{f}' \in \tilde{F}} N_{\tilde{q}}(\tilde{f}) \cdot (\chi(c_{\tilde{q}}(\tilde{f}), c_{\tilde{q}}(\tilde{f}')) N_{\tilde{q}}(\tilde{f}')). \end{aligned}$$

Note that  $\tilde{q}$  does not need to be consistent with  $q$ , and can be defined on a different set of indices,  $\tilde{M} = \{1, \dots, \tilde{m}\}$  and triangle structure  $\tilde{F}$ . One then has  $dU_q = \alpha_q \nu_M$ , where, as above,  $\nu_M$  is the counting measure on  $M$ , and

$$\alpha_q(i) = \sum_{f \in F, i \in f} (dZ_{c_q(f)}^T N_q(f)/3 + e_q(f, i) \times Z(c_q(f))),$$

with  $e_q(f, i) = q(k) - q(j)$  the oriented edge opposed to  $q(i)$  in  $q(f)$ , and

$$Z(\cdot) = \sum_{f \in F} \chi(\cdot, c_q(f)) N_q(f) - \sum_{\tilde{f} \in \tilde{F}} \chi(\cdot, c_{\tilde{q}}(\tilde{f})) N_{\tilde{q}}(\tilde{f}).$$

**A.3. Convergence of Discrete Currents Norms.** Let  $S = q(M)$  and  $\tilde{S}_1 = \tilde{q}(M)$  be two smooth embedded surfaces in  $\mathbb{R}^3$ , with  $M$  a surface with volume form  $\eta$ . Let  $q^{(\ell)}$  and  $\tilde{q}^{(\ell)}$ ,  $\ell = 0, 1, \dots$ , be sequences of triangulations of  $S$  and  $\tilde{S}$ , with set of faces respectively denoted by  $F_\ell$  and  $\tilde{F}_\ell$ .

Also let  $W$  be a reproducing kernel Hilbert space of vector fields on  $\mathbb{R}^3$  with kernel  $\chi$ , and assume these sequences of triangulations converge nicely to  $S_{init}$  and  $S_{target}$ . We will prove that

$$\|\mu_{q^{(\ell)}} - \mu_{\tilde{q}^{(\ell)}}\|_W^2 \rightarrow \|\mu_S - \mu_{\tilde{S}}\|_W^2$$

when  $\ell$  goes to infinity.

Indeed, for each face  $f$  (resp.  $\tilde{f}$ ) of each triangulation of  $S$  (resp.  $\tilde{S}$ ), let  $\tau_f$  be a geodesic triangle on  $S$  (resp.  $\tilde{S}$ ) with vertices  $q_j^{(\ell)}$ ,  $j \in f$  (resp.  $\tilde{q}_j^{(\ell)}$ ,  $j \in \tilde{f}$ ). For small enough triangles (i.e., big enough  $\ell$ ), the geodesic triangles  $\tau_f \subset S$ ,  $f \in F_\ell$ , form a partition of  $S$ , and the  $\tau_{\tilde{f}}$ ,  $\tilde{f} \in \tilde{F}_\ell$ , a partition of  $\tilde{S}$ , up to a zero measure set. We can then

write, for each  $\ell$  big enough, the value of  $U(q) - U_\ell(q^{(\ell)})$  as equal to

$$\begin{aligned} & \sum_{f \in F_\ell} \sum_{\tilde{f} \in \tilde{F}_\ell} \iint_{\tau_f \times \tau_{\tilde{f}}} \left( N_S(x) \cdot (\chi(x, y) N_S(y)) - \frac{N_{q^{(\ell)}}(f)}{\text{area}(\tau_f)} \cdot (\chi(c_{q^{(\ell)}}(f), c_{q^{(\ell)}}(\tilde{f}')) \frac{N_{q^{(\ell)}}(\tilde{f}')}{\text{area}(\tau_{\tilde{f}'})} \right) d\mathcal{A}_S(x) d\mathcal{A}_S(y) \\ & - 2 \sum_{f \in F_\ell} \sum_{\tilde{f} \in \tilde{F}_\ell} \iint_{\tau_f \times \tau_{\tilde{f}}} \left( N_S(x) \cdot (\chi(x, y) N_{\tilde{S}}(y)) - \frac{N_{q^{(\ell)}}(f)}{\text{area}(\tau_f)} \cdot (\chi(c_{q^{(\ell)}}(f), c_{\tilde{q}^{(\ell)}}(\tilde{f})) \frac{N_{\tilde{q}^{(\ell)}}(\tilde{f})}{\text{area}(\tau_{\tilde{f}})} \right) d\mathcal{A}_S(x) d\mathcal{A}_{\tilde{S}}(y) \\ & + \sum_{\tilde{f} \in \tilde{F}_\ell} \sum_{\tilde{f}' \in \tilde{F}'_\ell} \iint_{\tau_{\tilde{f}} \times \tau_{\tilde{f}'}} \left( N_{\tilde{S}}(x) \cdot (\chi(x, y) N_{\tilde{S}}(y)) - \frac{N_{\tilde{q}^{(\ell)}}(\tilde{f})}{\text{area}(\tau_{\tilde{f}})} \cdot (\chi(c_{\tilde{q}^{(\ell)}}(\tilde{f}), c_{\tilde{q}^{(\ell)}}(\tilde{f}')) \frac{N_{\tilde{q}^{(\ell)}}(\tilde{f}')}{\text{area}(\tau_{\tilde{f}'})} \right) d\mathcal{A}_{\tilde{S}}(x) d\mathcal{A}_{\tilde{S}}(y) \end{aligned}$$

But the nice convergence of the triangulations imply

$$\max_{f \in F_\ell} \left| \frac{\text{area}(q^{(\ell)}(f))}{\text{area}(\tau_f)} - 1 \right| \rightarrow 0, \quad \max_{f \in F_\ell} \max_{x \in \tau_f} \left| N_S(x) - \frac{N_{q^{(\ell)}}(f)}{\text{area}(q^{(\ell)}(f))} \right| \rightarrow 0,$$

along with

$$\max_{\tilde{f} \in \tilde{F}_\ell} \left| \frac{\text{area}(\tilde{q}^{(\ell)}(\tilde{f}))}{\text{area}(\tau_{\tilde{f}})} - 1 \right| \rightarrow 0, \quad \max_{\tilde{f} \in \tilde{F}_\ell} \max_{x \in \tau_{\tilde{f}}} \left| N_{\tilde{S}}(x) - \frac{N_{\tilde{q}^{(\ell)}}(\tilde{f})}{\text{area}(\tilde{q}^{(\ell)}(\tilde{f}))} \right| \rightarrow 0,$$

and

$$\max_{f \in F_\ell, \tilde{f} \in \tilde{F}_\ell} \max_{x \in \tau_f, y \in \tau_{\tilde{f}}} |\chi(x, y) - \chi(c_{q^{(\ell)}}(f), c_{\tilde{q}^{(\ell)}}(\tilde{f}))| \rightarrow 0$$

when  $\ell \rightarrow \infty$ . This implies that  $U(q) - U_\ell(q^{(\ell)})$  does go to zero as  $\ell$  goes to infinity.

## APPENDIX B. CONVERGENCE RESULTS FOR MINIMIZERS WITH SLIDING CONSTRAINTS

Here, we prove the weak convergence of solutions to the discrete sliding problem with relaxed constraints toward minimizers of the continuous sliding problem with equality constraints. We use the notations of Section 5.2. We begin by finding a candidate for the sequence of positive numbers  $(\varepsilon_\ell)_{\ell \in \mathbb{N}}$ .

*Step one: candidate for  $\varepsilon_\ell$ .* Let  $(v_1, \dots, v_n) \in L^2(0, 1; V_1 \times V_n)$  be minimizers of the cost with continuous sliding constraints, with flows  $(\varphi_1, \dots, \varphi_n)$ . In particular

$$E_* = \frac{1}{2} \sum_{k=1}^n \int_0^1 \|v_k(t)\|_{V_k}^2 dt + \sum_{k=0}^{n-1} \left( U_k(\varphi_k(1) \circ q_{init}^{(k)}) + \tilde{U}_k(\varphi_n(1) \circ q_{init}^{(k)}) \right)$$

is the minimum of the cost function with continuous sliding constraints.

Let  $x_j^{(k, \ell)}(t) = \varphi_k(t, x_{j, init}^{(k, \ell)})$ ,  $k = 1, \dots, n-1$ ,  $j = 1, \dots, l_{k, \ell}$  and  $t \mapsto z^{(\ell)}(t)$  be the deformations of the  $\ell$ -th triangulation vertices induced by  $(v_1, \dots, v_n)$ , and  $N^{(n, \ell)}(t, f)$ ,  $f \in F_{n, \ell}$ , the corresponding area-weighted normals. Thanks to condition (i) of nice convergence, each  $z_j^{(k, \ell)}(t)$  belongs to  $\varphi_n(t, S^k)$ . Hence, we have that, for almost every time  $t$ , and every  $k = 1, \dots, n-1$ ,

$$\max_{f \in F_{k, \ell}} \left| \frac{N^{(n, \ell)}(f)}{|N^{(n, \ell)}(f)|} \cdot \left( \sum_{j \in f} (v_k(z_j^{(k, \ell)}) - v_n(z_j^{(k, \ell)})) \right) \right|$$

is less than or equal to

$$\begin{aligned} (18) \quad & \max_{f \in F_{k, \ell}} \sum_{j \in f} \left| \left( \frac{N^{(n, \ell)}(f)}{|N^{(n, \ell)}(f)|} - N_{\varphi_n(S_{init}^k)}(z_j^{(k, \ell)}) \right) \cdot (v_k(z_j^{(k, \ell)}) - v_n(z_j^{(k, \ell)})) \right| \\ & + \max_{f \in F_{k, \ell}} \sum_{j \in f} \left| N_{\varphi_n(S_{init}^k)}(z_j^{(k, \ell)}) \cdot (v_k(z_j^{(k, \ell)}) - v_n(z_j^{(k, \ell)})) \right|. \end{aligned}$$

The second term in (18) is equal to 0, as we recognize the formula for continuous sliding constraints, which  $(v_k, k = 1, \dots, n)$  satisfies by construction.

For the other terms, remark that  $\sum_{k=1}^n \|v_k\|_{V_k}^2$  is constant, since the constraints are invariant by reparametrization. Since each  $V_k$  has continuous inclusion in  $C_0^2(\mathbb{R}^d, \mathbb{R}^d)$ , so there exists  $C > 0$  such that, for almost every  $t$ , and every  $y, y'$  in  $\mathbb{R}^d$ , we have

$$|v_n(t, y)| \leq C \|v\|_V, \quad |v(t, y) - v(t, y')| \leq C \|v\|_V |y - y'|.$$

Then, Gronwall's lemma ensures (increasing  $C$  if needed), that  $|\varphi_n(t, y) - \varphi_n(t, y')| \leq C|y - y'|$ , and the same is true for  $d\varphi(t)$ .

This shows that the first term of (18) is less than or equal to

$$\begin{aligned} 2C \max_{f \in F_{k,\ell}} \sum_{j \in f} \left| N_{\varphi_n(S_{init}^k)}(z_j^{(k,\ell)}) - \frac{N^{(n,\ell)}(f)}{|N^{(n,\ell)}(f)|} \right| &\leq 2C \max_{f \in F_{k,\ell}} \sum_{j \in f} \left| N_{\varphi_n(S_{init}^k)}(z_j^{(k,\ell)}) - \frac{d\varphi_n(z_{j,init}^{(k,\ell)})^{-T} N^{(n,\ell)}(f)}{|d\varphi_n(z_{j,init}^{(k,\ell)})^{-T} N^{(n,\ell)}(f)|} \right| \\ &+ \max_{f \in F_{k,\ell}} \sum_{j \in f} \left| \frac{d\varphi_n(z_{j,init}^{(k,\ell)})^{-T} N^{(n,\ell)}(f)}{|d\varphi_n(z_{j,init}^{(k,\ell)})^{-T} N^{(n,\ell)}(f)|} - \frac{N^{(n,\ell)}(f)}{|N^{(n,\ell)}(f)|} \right| \\ &\leq 2C^2 \max_{f \in F_{k,\ell}} \sum_{j \in f} \left| N_{S_{init}^k}(z_{j,init}^{(k,\ell)}) - \frac{N_{init}^{(n,\ell)}(f)}{|N_{init}^{(n,\ell)}(t, f)|} \right| \\ &+ \max_{f \in F_{k,\ell}} \sum_{j \in f} \left| \frac{d\varphi_n(z_{j,init}^{(k,\ell)})^{-T} N_{init}^{(n,\ell)}(f)}{|d\varphi_n(z_{j,init}^{(k,\ell)})^{-T} N_{init}^{(n,\ell)}(f)|} - \frac{N^{(n,\ell)}(f)}{|N^{(n,\ell)}(f)|} \right|. \end{aligned}$$

The first term after this last inequality goes to 0 as  $\ell$  goes to infinity thanks to the convergence of normals (Property (v) of a nice convergence). A straightforward computation and, again, Gronwall's lemma, shows that

$$\max_{f \in F_{k,\ell}} \left| \frac{d\varphi_n(t, z_{j,init}^{(k,\ell)})^{-T} N_{init}^{(n,\ell)}(f)}{|d\varphi_n(t, z_{j,init}^{(k,\ell)})^{-T} N_{init}^{(n,\ell)}(f)|} - \frac{N^{(n,\ell)}(t, f)}{|N^{(n,\ell)}(t, f)|} \right| \leq C \max_{f \in F_{k,\ell}} \eta(k, \ell, f).$$

Consequently, there exists a sequence  $(\varepsilon_\ell)_{\ell \in \mathbb{N}}$ , going to 0 at infinity, such that any minimizer of the continuous sliding problem satisfies the relaxed constraints

$$\max_{f \in F_{k,\ell}} \left| N^{(n,\ell)}(f) \cdot \left( \sum_{j \in f} (v_k(z_j^{(k,\ell)}) - v_n(z_j^{(k,\ell)})) \right) \right| \leq \varepsilon_\ell |N^{(n,\ell)}(f)|.$$

*Step two: weak convergence.* Now let  $(v_{k,\ell}, k = 1, \dots, n)_{\ell \in \mathbb{N}}$  be a sequence of minimizers of the discretized sliding problem with relaxed constraints

$$\max_{f \in F_{k,\ell}} \left| N^{(n,\ell)}(f) \cdot \left( \sum_{j \in f} (v_{k,\ell}(z_j^{(k,\ell)}) - v_{n,\ell}(z_j^{(k,\ell)})) \right) \right| \leq \varepsilon_\ell |N^{(n,\ell)}(f)|.$$

Denote by  $\varphi_{k,\ell}$  their respective flows. Thanks to the convergence of current norms for nicely converging triangulations, we see that each sequence  $(v_{k,\ell})_{\ell \in \mathbb{N}}$  is bounded in  $L^2(0, 1; V_k)$ . Hence, up to the extraction of a subsequence, we have, for each  $k$ , that  $v_{k,\ell}$  converges weakly toward some limit  $v_k^*$  in  $L^2(0, 1; V_K)$  with flow  $\varphi_{k,*}$ . This implies that  $\varphi_{k,\ell}$  and  $d\varphi_{k,\ell}$  converge strongly toward  $\varphi_{k,*}$  and  $d\varphi_{k,*}$  in some compact subset  $K$  that includes  $\cup_{k=1}^{n-1} S_{init}^k$ .

The triangulation is nested (Assumption (ii) of a nice convergence), so we can order the components of each  $z^{(k,\ell)}$  so that

$$z^{(k,\ell+1)} = (z_1^{(k,\ell)}, \dots, z_{l_{k,\ell}}^{(k,\ell)}; z_{l_{k,\ell}+1}^{(k,\ell+1)}, \dots, z_{l_{k,\ell+1}}^{(k,\ell+1)})$$

for every integer  $\ell$ . We start by proving that, for each  $i$ , we have

$$N_{\varphi_n(t, S_{init}^k)}(z_i^{(k,*)})(t) \cdot v_{k,*}(t, z_i^{(k,*)})(t) = 0$$

for almost every  $t$ , where  $z_i^{(k,*)}(t) = \varphi_{n,*}(t, z_{init,i}^{(k,*)})$ . Fix some integer  $i$ . Choose, for each  $\ell$  in  $\mathbb{N}$ , two integers  $j_\ell$  and  $j'_\ell$  such that  $i, j_\ell$ , and  $j'_\ell$  belong to a face  $f_\ell \in F_{k,\ell}$ . Consider the sequence in  $L^2(0, 1; \mathbb{R})$  of functions

$$c_\ell : t \mapsto \frac{N^{(n,\ell)}(t, f_\ell)}{|N^{(n,\ell)}(t, f_\ell)|} \cdot (\delta v_{k,\ell}(t, z_i^{(k,\ell)}(t)) + \delta v_{k,\ell}(t, z_{j'_\ell}^{(k,\ell)}(t)) + \delta v_{k,\ell}(t, z_{j_\ell}^{(k,\ell)}(t))),$$

where  $\delta v_{k,\ell}(t, x) = v_{k,\ell}(t, x) - v_{n,\ell}(t, x)$ . By construction, for any  $\varepsilon > 0$ , and for any  $\ell$  big enough,  $-\varepsilon \leq c_\ell(t) \leq \varepsilon$  almost everywhere. Since  $L^2(0, 1; [-\varepsilon, \varepsilon])$  is weakly compact in  $L^2(0, 1; \mathbb{R})$  and goes to  $\{0\}$  as  $\varepsilon$  goes to 0, we see that  $c_\ell$  goes weakly to 0 as  $\ell$  goes to infinity.

On the other hand, we can prove that  $c_\ell$  converges weakly to  $t \mapsto 3N_{\varphi_n(t, S_{init}^k)}(z_i^{(k,*)})(t) \cdot v_{k,*}(t, z_i^{(k,*)})(t)$ . Indeed, omitting  $t$  for readability, we also have

$$\begin{aligned} c_\ell &= \left( \frac{N^{(n,\ell)}(f_\ell)}{|N^{(n,\ell)}(f_\ell)|} - N_{\varphi_{n,*}(S_{init}^k)}(z_i^{(k,*)}) \right) \cdot (\delta v_{k,\ell}(z_i^{(k,\ell)}) + \delta v_{k,\ell}(z_{j'_\ell}^{(k,\ell)}) + \delta v_{k,\ell}(z_{j_\ell}^{(k,\ell)})) \\ &+ N_{\varphi_{n,*}(S_{init}^k)}(z_i^{(k,*)}) \cdot (\delta v_{k,\ell}(z_i^{(k,\ell)}) + \delta v_{k,\ell}(z_{j'_\ell}^{(k,\ell)}) + \delta v_{k,\ell}(z_{j_\ell}^{(k,\ell)})). \end{aligned}$$

Let us now prove that  $\delta v_{k,\ell}(z_i^{(k,\ell)})$ ,  $\delta v_{k,\ell}(z_{j'_\ell}^{(k,\ell)})$ , and  $\delta v_{k,\ell}(z_{j_\ell}^{(k,\ell)})$  each converges weakly toward  $\delta v_{k,*}(z_i^{(k,*)}) = v_{k,*}(z_i^{(k,*)}) - v_{n,*}(z_i^{(k,*)})$  in  $L^2(0, 1; \mathbb{R}^3)$ . We only do it for  $j_\ell$ , the case for the other two being either similar or easier. We have

$$\delta v_{k,\ell}(z_{j'_\ell}^{(k,\ell)}) = (\delta v_{k,\ell}(z_{j'_\ell}^{(k,\ell)}) - \delta v_{k,\ell}(z_i^{(k,*)})) + \delta v_{k,\ell}(z_i^{(k,*)})$$

Now, for any  $\psi \in L^2(0, 1; \mathbb{R}^3)$ , we have

$$\int_{[0,1]} |\delta v_{k,\ell}(z_{j'_\ell}^{(k,\ell)}) - \delta v_{k,\ell}(z_i^{(k,*)})|^2 \leq C \max_{t \in [0,1]} |z_{j'_\ell}^{(k,\ell)}(t) - z_i^{(k,*)}(t)|^2 \int_{[0,1]} (\|v_{k,\ell}\|_{V_k}^2 + \|v_{n,\ell}\|_{V_n}^2) \leq C^2 \eta(k, \ell, f_\ell) \int_{[0,1]} (\|v_{k,\ell}\|_{V_k}^2 + \|v_{n,\ell}\|_{V_n}^2)$$

which clearly goes to 0 as  $\ell$  goes to infinity. On the other hand,  $\delta v_{k,\ell}(z_i^{(k,*)})$  converges weakly to  $\delta v_{k,*}(z_i^{(k,*)})$  as  $\ell$  goes to infinity. Indeed, for any  $\psi \in L^2(0, 1; \mathbb{R})$ , the mapping

$$v \in L^2(0, 1; V_k), v' \in L^2(0, 1; V_n) \mapsto \int_0^1 \psi(t) \cdot (v(t, z_i^{k,*}(t)) - v'(t, z_i^{k,*}(t))) dt$$

is a continuous linear form, and  $(v_{k,\ell}, v_{n,\ell})$  converges weakly to  $(v_{k,*}, v_{n,*})$ . Hence, we get that  $\delta v_{k,\ell}(z_{j'_\ell}^{(k,\ell)})$  converges weakly to  $\delta v_{k,*}(z_i^{(k,*)})$ , and the same is true for  $\delta v_{k,\ell}(z_{j'_\ell}^{(k,\ell)})$  and  $\delta v_{k,\ell}(z_{j_\ell}^{(k,\ell)})$ .

Now the strong convergence of  $\frac{N^{(n,\ell)}(f_\ell)}{|N^{(n,\ell)}(f_\ell)|}$  toward  $N_{\varphi_{n,*}(S_{init}^k)}(z_i^{(k,*)})$  in  $L^2(0, 1; \mathbb{R}^3)$  (and even in  $C^0(0, 1; \mathbb{R})$ ) is an immediate consequence of the nice convergence of the triangulations and the strong convergence of the flows  $\varphi_{k,\ell}$  toward  $\varphi_{k,*}$ . Therefore, we get  $c_\ell$  converges weakly in  $L^2(0, 1; \mathbb{R})$  to

$$t \mapsto 3N_{\varphi_n(t, S_{init}^k)}(z_i^{(k,*)})(t) \cdot v_{k,*}(t, z_i^{(k,*)})(t).$$

By unicity of the weak limit value of a sequence, we get, for almost every  $t$  in  $[0, 1]$ ,

$$N_{\varphi_n(t, S_{init}^k)}(z_i^{(k,*)})(t) \cdot v_{k,*}(t, z_i^{(k,*)})(t) = 0.$$

Hence, for any  $i \in \mathbb{N}$  and almost every  $t$  in  $[0, 1]$ , we have

$$N_{\varphi_n(t, S_{init}^k)}(z_i^{(k,*)})(t) \cdot v_{k,*}(t, z_i^{(k,*)})(t) = 0.$$

But  $\mathbb{N}$  is countable, so we can write, for almost every  $t$  in  $[0, 1]$ ,

$$\forall i \in \mathbb{N}, \quad N_{\varphi_n(t, S_{init}^k)}(z_i^{(k,*)})(t) \cdot v_{k,*}(t, z_i^{(k,*)})(t) = 0.$$

But, by nice convergence, we know that for every  $t$ ,  $\{z_i^{(k,*)}(t), i \in \mathbb{N}\}$  is dense in  $\varphi_n(t, S_{init}^k)$ . Moreover,  $v_{k*}(t)$  and  $N_{\varphi_n(t, S_{init}^k)}$  are continuous on  $\varphi_n(t, S_{init}^k)$  for almost every  $t$ .

We get, for almost every  $t$  in  $[0, 1]$

$$\forall x \in \varphi_n(t, S_{init}^k), \quad N_{\varphi_n(t, S_{init}^k)}(x) \cdot v_{k*}(t, x) = 0.$$

Since this is true for each  $k = 1, \dots, n-1$ , we see that  $(v_{k*}, k = 1, \dots, n)$  does satisfy the sliding constraints for the continuous problem.

*Step 3: minimality.* From the nice convergence of the triangulations involved, and the strong  $\mathcal{C}^1$ -convergence of the flows, we easily deduce from Appendix A.3 that each  $U_{k,\ell}(\varphi_{k,\ell} \circ q_{init}^{(k,\ell)})$  and  $\tilde{U}_{k,\ell}(\varphi_{n,\ell} \circ q_{init}^{(n,k,\ell)})$  converge respectively to  $U_k(\varphi_{k,*} \circ q_{init}^{(k)})$  and  $\tilde{U}_k(\varphi_{n,*} \circ q_{init}^{(k)})$ . Therefore, because of the properties of the weak convergence, we have

$$\begin{aligned} E_* &\leq \sum_{k=1}^n \int_0^1 \|v_{k*}(t)\|_{V_k}^2 dt + \sum_{k=1}^{n-1} (U_k(\varphi_{k,*} \circ q_{init}^{(k)}) + \tilde{U}_k(\varphi_{n,*} \circ q_{init}^{(k)})) \\ &\leq \liminf_{\ell} \sum_{k=1}^n \int_0^1 \|v_{k,\ell}(t)\|_{V_k}^2 dt + \sum_{k=1}^{n-1} (U_{k,\ell}(\varphi_{k,\ell} \circ q_{init}^{(k,\ell)}) + \tilde{U}_{k,\ell}(\varphi_{n,\ell} \circ q_{init}^{(k,\ell)})). \end{aligned}$$

But because of Step 1 of this proof and the construction of each  $(v_{k,\ell}, k = 1, \dots, n)$ , we have, for every integer  $\ell$ ,

$$E_* \geq \sum_{k=1}^n \int_0^1 \|v_{k,\ell}(t)\|_{V_k}^2 dt + \sum_{k=1}^{n-1} (U_{k,\ell}(\varphi_{k,\ell} \circ q_{init}^{(k,\ell)}) + \tilde{U}_{k,\ell}(\varphi_{n,\ell} \circ q_{init}^{(k,\ell)})),$$

so

$$E_* = \sum_{k=1}^n \int_0^1 \|v_{k*}(t)\|_{V_k}^2 dt + \sum_{k=1}^{n-1} (U_k(\varphi_{k,*} \circ q_{init}^{(k)}) + \tilde{U}_k(\varphi_{n,*} \circ q_{init}^{(k)})),$$

which completes the proof.

#### APPENDIX C. DERIVATIVES OF THE AUGMENTED LAGRANGIAN

We give the formulas for the differentials required to implement the augmented Lagrangian method.

*Identity Constraints.* For identity constraints, we use the notations of Section 4.2. We then want to minimize

$$E_{\lambda,\mu}(\alpha, \beta, x, z) = \int_0^1 L_{\lambda(t),\mu}(\alpha(t)\beta(t), x(t), z(t)) dt + \sum_{k=1}^{n-1} U_k(x^{(k)}(1)) + \sum_{k=1}^{n-1} \tilde{U}_k(z^{(k)}(1)),$$

where

$$L_{\lambda,\mu} = \frac{1}{2} \sum_{k=1}^{n-1} \alpha^{(k)} \cdot (K^{(k)}(x^{(k)})\alpha^{(k)}) + \frac{1}{2} \beta \cdot (K^{(n)}(z)\beta) - \sum_{k=1}^{n-1} \lambda^{(k)} \cdot (x^{(k)} - z^{(k)}) + \frac{\mu}{2} \sum_{k=1}^{n-1} |x^{(k)} - z^{(k)}|^2,$$

over controls  $\alpha$  and  $\beta$  subject almost everywhere along  $[0, 1]$  to

$$\begin{cases} \partial_t x^{(k)} = K^{(k)}(x^{(k)})\alpha^{(k)}, \\ \partial_t z = K^{(n)}(z)\beta. \end{cases}$$

For this, we use the Hamiltonian method described in Section 2.2. Denoting the co-states by  $p^{x,k}$ ,  $k = 1, \dots, n-1$ , and  $p^z$ , the associated Hamiltonian is

$$H(t, x, z, p^x, p^z, \alpha, \beta) = \sum_{k=1}^{n-1} p^{x,k} \cdot K^{(k)}(x^{(k)})\alpha^{(k)} + p^z \cdot K^{(n)}(z)\beta - L_{\lambda(t),\mu}.$$

Given  $\alpha$  and  $\beta$  and the associated trajectories  $x$  and  $z$ , one has to solve the adjoint equations

$$\begin{aligned}\partial_t p^{x,k} &= -\partial_{x^{(k)}} H, & p^{x,k}(1) &= -\nabla U_k(x^{(k)}(1)), & k &= 1, \dots, n-1, \\ \partial_t p^z &= -\partial_z H, & p^z(1) &= -\nabla \tilde{U}_k(z^{(k)}(1)), & k &= 1, \dots, n-1.\end{aligned}$$

The computation of the differential system gives

$$\begin{aligned}\partial_t p_i^{x,k} &= -\sum_{j=1}^{m_k} \nabla_1(p_i^{x,k} \cdot K^{(k)}(x_i^{(k)}, x_j^{(k)}) \alpha_j^{(k)}) - \sum_{j=1}^{m_k} \nabla_1(\alpha_i^{(k)} \cdot K^{(k)}(x_i^{(k)}, x_j^{(k)}) p_j^{x,k}) \\ &\quad + 2 \sum_{j=1}^{m_k} \nabla_1(\alpha_i^{(k)} \cdot K^{(k)}(x_i^{(k)}, x_j^{(k)}) \alpha_j^{(k)}) - (\lambda^{(k)} - \mu(x^{(k)} - z^{(k)})),\end{aligned}$$

and

$$\begin{aligned}\partial_t p_i^{z,k} &= -\sum_{l=1}^{n-1} \sum_{j=1}^{m_l} \nabla_1(p_i^{z,k} \cdot K^{(n)}(z_i^{(k)}, z_j^{(l)}) \beta_j^{(l)}) - \sum_{l=1}^{n-1} \sum_{j=1}^{m_l} \nabla_1(\beta_i^{(k)} \cdot K^{(n)}(z_i^{(k)}, z_j^{(l)}) p_j^{z,l}) \\ &\quad + 2 \sum_{l=1}^{n-1} \sum_{j=1}^{m_l} \nabla_1(\beta_i^{(k)} \cdot K^{(n)}(z_i^{(k)}, z_j^{(l)}) \beta_j^{(l)}) + \sum_{l=1}^n (\lambda^{(l)} - \mu(x^{(l)} - z^{(l)}))\end{aligned}$$

The gradient of  $E_{\lambda,\mu}$  with respect to  $(\alpha, \beta)$  is then deduced from the partial differentials of  $H$  with respect to these variables, yielding

$$\begin{aligned}\nabla_{\alpha^{(k)}} E_{\lambda,\mu} &= K^{(k)}(x^{(k)})(\alpha^{(k)} - p^{x,k}), \\ \nabla_{\beta} E_{\lambda,\mu} &= K^{(n)}(z)(\beta - p^z).\end{aligned}$$

for the gradient with respect to the Hilbert product associated to the Euclidean metric. Another way is to compute the gradient with respect to the Hilbert metric described at the end of Section 2.2, in which case we obtain

$$\begin{aligned}\nabla_{\alpha^{(k)}} E_{\lambda,\mu} &= \alpha^{(k)} - p^{x,k}, \\ \nabla_{\beta} E_{\lambda,\mu} &= \beta - p^z.\end{aligned}$$

We found the latter method to converge more quickly in practical applications.

*Sliding constraints.* Here, we use the notations from Section 4.3. The functional we want to minimize is

$$(19) \quad E'_{\lambda,\mu}(\alpha, \beta, x, z) = \int_0^1 L'_{\lambda(t),\mu}(\alpha(t), \beta(t), x(t), z(t)) dt + \sum_{k=1}^{n-1} U_k(x^{(k)}(1)) + \sum_{k=1}^{n-1} \tilde{U}_k(z^{(k)}(1))$$

, with

$$L_{\lambda,\mu} = \frac{1}{2} \sum_{k=1}^{n-1} \alpha^{(k)} \cdot (K^{(k)}(x^{(k)}) \alpha^{(k)}) + \frac{1}{2} \beta \cdot (K^{(n)}(z) \beta) - \sum_{k=1}^{n-1} \sum_{f \in F_k} (\lambda_f \Gamma_f^{(k)}(x^{(k)}, z) - \frac{\mu}{2} \Gamma_f^{(k)}(x^{(k)}, z)^2).$$

We now compute the evolution equations for the co-states, as done with identity constraints. For  $f \in F_k$  and  $i \in M_k$ , we have

$$(20) \quad \partial_{x_i^{(k)}} \Gamma_f^{(k)} = \sum_{j \in f} \nabla_1(\alpha_i^{(k)} \cdot K^{(k)}(x_i^{(k)}, z_j^{(k)}) \tilde{N}^{(n)}(f)).$$

Denoting

$$\delta^{(k)}(f) := \sum_{j \in f} (u_k(z_j^{(k)}) - u_n(z_j^{(k)})),$$

if  $i \in f \in F_k$ , then

$$(21) \quad \partial_{z_i^{(k)}} \Gamma_f^{(k)} = -e_{i,f} \times \delta^{(k)}(f) - \sum_{l=1}^{n-1} \sum_{j=1}^{m_l} \nabla_1(\tilde{N}^{(n)}(f) \cdot K^{(n)}(z_i^{(k)}, z_j^{(l)}) \beta_j^{(l)}) \\ + \sum_{j=1}^{m_k} \nabla_1(\tilde{N}^{(n)}(f) \cdot K^{(k)}(z_i^{(k)}, x_j^{(k)}) \alpha_j^{(k)}) - \sum_{l=1}^{n-1} \sum_{j=1}^{m_l} \nabla_1(\beta_i^{(k)} \cdot K^{(n)}(z_i^{(k)}, z_j^{(l)}) \tilde{N}^{(n)}(f)).$$

Let  $p^{x,1}, \dots, p^{x,n-1}$  and  $p^z = (p^{z,1}, \dots, p^{z,n-1})$  be the co-states. Let  $\gamma_f^{(k)} = \lambda_f - \mu \Gamma_f^{(k)}$ . For  $i \in M_k$ , let  $F_k(i) = \{f \in M_k : i \in f\}$ . Then

$$\partial_t p_i^{x,k} = - \sum_{j=1}^{N_k} \nabla_1(p_i^{x,k} \cdot K^{(k)}(x_i^{(k)}, x_j^{(k)}) \alpha_j^{(k)}) - \sum_{j=1}^{N_k} \nabla_1(\alpha_i^{(k)} \cdot K^{(k)}(x_i^{(k)}, x_j^{(k)}) p_j^{x,k}) \\ + 2 \sum_{j=1}^{N_k} \nabla_1(\alpha_i^{(k)} \cdot K^{(k)}(x_i^{(k)}, x_j^{(k)}) \alpha_j^{(k)}) - \sum_{f \in F_k} \gamma_f^{(k)} \partial_{x_i^{(k)}} \Gamma_f^{(k)},$$

and

$$\partial_t p_i^{z,k} = - \sum_{j=1}^N \nabla_1(p_i^{z,i} \cdot K^{(n)}(z_i^{(k)}, z_j) \beta_j) - \sum_{j=1}^N \nabla_1(\beta_i^{(k)} \cdot K^{(n)}(z_i^{(k)}, z_j) p_j^z) \\ + 2 \sum_{j=1}^N \nabla_1(\beta_i^{(k)} \cdot K^{(n)}(z_i^{(k)}, z_j) \beta_j) - \sum_{f \in F_k} \gamma_f^{(k)} \partial_{z_i^{(k)}} \Gamma_f^{(k)},$$

where  $\partial_{x_i^{(k)}} \Gamma_f^{(k)}$  and  $\partial_{z_i^{(k)}} \Gamma_f^{(k)}$  are given by (20) and (21).

For  $f \in F_k$  ( $k = 1, \dots, n-1$ ), we have

$$\partial_{\alpha^{(k)}} \Gamma_f^{(k)} = \sum_{j \in f} K^{(k)}(x^{(k)}, z_j^{(k)}) \tilde{N}_j^{(n)}(f), \\ \partial_{\beta} \Gamma_f^{(k)} = - \sum_{j \in f} K^{(n)}(z, z_j^{(k)}) \tilde{N}_j^{(n)}(f),$$

Letting  $\theta_j^{(k)} = \sum_{f \in F_k: j \in f} \gamma_f^{(k)} \tilde{N}_j^{(n)}(f)$ , the gradient of  $E_{\lambda, \mu}$  in  $\alpha$  and in  $\beta$  with respect to the canonical  $L^2$  Hilbert product is then given by

$$\nabla_{\alpha^{(k)}} E_{\lambda, \mu} = K^{(k)}(x^{(k)}) (\alpha^{(k)} - p^{x,k}) - K^{(k)}(x^{(k)}, z) \theta, \\ \nabla_{\beta} E_{\lambda, \mu} = K^{(n)}(z) (\beta - p^z) + K^{(n)}(z, z) \theta$$

Another method is to take the Hilbert gradient with respect to the product introduced at the end of Section 2.2, which yields

$$\nabla_{\alpha^{(k)}} E_{\lambda, \mu} = \alpha^{(k)} - p^{x,k} - K^{(k)}(x^{(k)})^{-1} K^{(k)}(x^{(k)}, z) \theta, \\ \nabla_{\beta} E_{\lambda, \mu} = \beta - p^z + K^{(n)}(z, z) \theta.$$

In spite of it requiring the inversion of a linear system in the first equation, we found the latter version preferable to the  $L^2$  gradient in our experiments.

*A Remark: Kernel derivatives.* Expressions similar to  $\nabla_1(n \cdot K(x, y)\alpha)$  appear at multiple times in the previous computation (for some vectors  $n$  and  $\alpha$ ). For radial kernels ( $K(x, y) = G(|x - y|^2)\text{Id}_{\mathbb{R}^d}$ ), we have

$$\nabla_1(n \cdot K(x, y)\alpha) = 2G'(|x - y|^2)(n \cdot \alpha)(x - y),$$

which (slightly) simplifies the expressions.

## REFERENCES

- [1] Siamak Ardekani, Robert G Weiss, Albert C Lardo, Richard T George, Joao AC Lima, Katherine C Wu, Michael I Miller, Raimond L Winslow, and Laurent Younes. Cardiac motion analysis in ischemic and non-ischemic cardiomyopathy using parallel transport. In *Biomedical Imaging: From Nano to Macro, 2009. ISBI'09. IEEE International Symposium on*, pages 899–902. IEEE, 2009.
- [2] Sylvain Arguillère, Emmanuel Trélat, Alain Trouvé, and Laurent Younes. Shape deformation analysis from the optimal control viewpoint. *preprint arXiv:1401.0661*, to appear in *J. Math. Pures Appl.*, 2014.
- [3] John Ashburner. A fast diffeomorphic image registration algorithm. *Neuroimage*, 38(1):95–113, 2007.
- [4] John Ashburner and Karl J Friston. Diffeomorphic registration using geodesic shooting and Gauss–Newton optimisation. *Neuroimage*, 55(3):954–967, 2011.
- [5] Brian B Avants, P Thomas Schoenemann, and James C Gee. Lagrangian frame diffeomorphic image registration: Morphometric comparison of human and chimpanzee cortex. *Medical image analysis*, 10(3):397–412, 2006.
- [6] Robert Azencott, Roland Glowinski, Jiwen He, Aarti Jajoo, Yipeng Li, Andrey Martynenko, Ronald HW Hoppe, Sagit Benzekry, and Stuart H Little. Diffeomorphic matching and dynamic deformable surfaces in 3d medical imaging. *Comput. Methods Appl. Math.*, 10(3):235–274, 2010.
- [7] Ruzena Bajcsy, Robert Lieberman, and Martin Reivich. A computerized system for the elastic matching of deformed radiographic images to idealized atlas images. *Journal of Computer Assisted Tomography*, 7(4):618–625, 1983.
- [8] M Faisal Beg, Michael I Miller, Alain Trouvé, and Laurent Younes. Computing large deformation metric mappings via geodesic flows of diffeomorphisms. *International Journal of Computer Vision*, 61(2):139–157, 2005.
- [9] Martins Bruveris, François Gay-Balmaz, Darryl D Holm, and Tudor S Ratiu. The momentum map representation of images. *Journal of nonlinear science*, 21(1):115–150, 2011.
- [10] Yan Cao, Michael I Miller, Raimond L Winslow, and Laurent Younes. Large deformation diffeomorphic metric mapping of vector fields. *IEEE Transactions on Medical Imaging*, 24(9):1216–1230, 2005.
- [11] Can Ceritoglu, Kenichi Oishi, Xin Li, Ming-Chung Chou, Laurent Younes, Marilyn Albert, Constantine Lyketsos, Peter van Zijl, Michael I Miller, and Susumu Mori. Multi-contrast large deformation diffeomorphic metric mapping for diffusion tensor imaging. *Neuroimage*, 47(2):618–627, 2009.
- [12] Gary E. Christensen, Richard D. Rabbitt, and Michael I. Miller. Deformable templates using large deformation kinematics. *IEEE Transactions on Image Processing*, 5(10):1435–1447, 1996.
- [13] CJ Cotter and DD Holm. Discrete momentum maps for lattice epdiff. In Temam and Tribbia, editors, *Handbook of Numerical Analysis*, pages 247–278. North-Holland, 2009.
- [14] Colin J Cotter and Darryl D Holm. Singular solutions, momentum maps and computational anatomy. *arXiv preprint nlin/0605020*, 2006.
- [15] WR Crum, T Hartkens, and DLG Hill. Non-rigid image registration: theory and practice. *British Journal of Radiology*, 77(suppl 2):S140–S153, 2004.
- [16] Marc Droske and Martin Rumpf. A variational approach to nonrigid morphological image registration. *SIAM Journal on Applied Mathematics*, 64(2):668–687, 2004.
- [17] P Dupuis, U Grenander, and MI Miller. Variation Problems on Flows of Diffeomorphisms for Image Matching. *Quarterly of Applied Mathematics*, LVI(4):587–600, 1998.
- [18] Stanley Durrleman, Stéphanie Allasonnière, and Sarang Joshi. Sparse adaptive parameterization of variability in image ensembles. *International Journal of Computer Vision*, 101(1):161–183, 2013.
- [19] Stanley Durrleman, Xavier Pennec, Alain Trouvé, Guido Gerig, and Nicholas Ayache. Spatiotemporal atlas estimation for developmental delay detection in longitudinal datasets. In *Medical Image Computing and Computer-Assisted Intervention—MICCAI 2009*, pages 297–304. Springer, 2009.
- [20] Herbert Federer and Herbert Federer. *Geometric measure theory*, volume 1996. Springer New York, 1969.
- [21] Joan Glaunès, Anqi Qiu, Michael I Miller, and Laurent Younes. Large deformation diffeomorphic metric curve mapping. *International journal of computer vision*, 80(3):317–336, 2008.
- [22] Joan Glaunès, Marc Vaillant, and Michael I Miller. Landmark Matching via Large Deformation Diffeomorphisms on the Sphere. *Journal of Mathematical Imaging and Vision*, 20:179–200, 2004.
- [23] Ben Glocker, Nikos Komodakis, Georgios Tziritas, Nassir Navab, and Nikos Paragios. Dense image registration through mrfs and efficient linear programming. *Medical image analysis*, 12(6):731–741, 2008.
- [24] A Ardeshir Goshtasby. *Image Registration: Principles, Tools and Methods*. Springer, 2012.
- [25] Ulf Grenander. *General pattern theory: A mathematical study of regular structures*. Clarendon Press Oxford, 1993.

- [26] Xianfeng Gu, Yalin Wang, Tony F Chan, Paul M Thompson, and Shing-Tung Yau. Genus zero surface conformal mapping and its application to brain surface mapping. In *Information Processing in Medical Imaging*, pages 172–184. Springer, 2003.
- [27] Xianfeng Gu, Yalin Wang, Tony F. Chan, Paul M. Thompson, and Shing-Tung Yau. Genus zero surface conformal mapping and its application to brain surface mapping. *IEEE Transactions on Medical Imaging*, 23(8):949–958, 2004.
- [28] Andreas Günther, Hans Lamecker, and Martin Weiser. Flexible shape matching with finite element based lddmm. *International Journal of Computer Vision*, pages 1–16, 2012.
- [29] Andreas Günther, Hans Lamecker, Martin Weiser, et al. Direct lddmm of discrete currents with adaptive finite elements. In *Proceedings of the Third International Workshop on Mathematical Foundations of Computational Anatomy-Geometrical and Statistical Methods for Modelling Biological Shape Variability*, pages 1–14, 2011.
- [30] Eldad Haber, Gallagher Pryor, John Melonakos, Allen Tannenbaum, et al. 3d nonrigid registration via optimal mass transport on the gpu. *Medical image analysis*, 13(6):931–940, 2009.
- [31] Steven Haker, Sigurd Angenent, Allen Tannenbaum, Ron Kikinis, Guillermo Sapiro, and Michael Halle. Conformal surface parameterization for texture mapping. *IEEE Transactions on Visualization and Computer Graphics*, 6(2):181–189, 2000.
- [32] Steven Haker, Lei Zhu, Allen Tannenbaum, and Sigurd Angenent. Optimal mass transport for registration and warping. *International Journal of Computer Vision*, 60(3):225–240, 2004.
- [33] Monica K Hurdal, Philip L Bowers, Ken Stephenson, L Sumners De Witt, Kelly Rehm, Kirt Schaper, and David A Rottenberg. Quasi-conformally flat mapping the human cerebellum. In *Medical Image Computing and Computer-Assisted Intervention–MICCAI99*, pages 279–286. Springer, 1999.
- [34] Monica K Hurdal and Ken Stephenson. Cortical cartography using the discrete conformal approach of circle packings. *Neuroimage*, 23:S119–S128, 2004.
- [35] Monica K Hurdal and Ken Stephenson. Discrete conformal methods for cortical brain flattening. *Neuroimage*, 45(1):S86–S98, 2009.
- [36] Monica K Hurdal, Ken Stephenson, Phil Bowers, De Witt Sumners, and David A Rottenberg. Coordinate systems for conformal cerebellar flat maps. *Neuroimage*, 11(5):S467, 2000.
- [37] Miao Jin, Yalin Wang, S-T Yau, and Xianfeng Gu. Optimal global conformal surface parameterization. In *Visualization, 2004. IEEE*, pages 267–274. IEEE, 2004.
- [38] Sarang C. Joshi and Michael I. Miller. Landmark matching via large deformation diffeomorphisms. *IEEE Transactions on Image Processing*, 9:1357–1370, 2000.
- [39] Yaron Lipman and Ingrid Daubechies. Surface comparison with mass transportation. *arXiv preprint arXiv:0912.3488*, 2009.
- [40] Yaron Lipman and Ingrid Daubechies. Conformal wasserstein distances: Comparing surfaces in polynomial time. *Advances in Mathematics*, 227(3):1047–1077, 2011.
- [41] Lok Ming Lui, Tsz Wai Wong, Paul Thompson, Tony Chan, Xianfeng Gu, and Shing-Tung Yau. Shape-based diffeomorphic registration on hippocampal surfaces using Beltrami holomorphic flow. In *Medical Image Computing and Computer-Assisted Intervention–MICCAI 2010*, pages 323–330. Springer, 2010.
- [42] Facundo Mémoli. On the use of gromov-hausdorff distances for shape comparison. In *Eurographics symposium on point-based graphics*, pages 81–90. The Eurographics Association, 2007.
- [43] Facundo Mémoli. Gromov-wasserstein distances and the metric approach to object matching. *Foundations of Computational Mathematics*, 11(4):417–487, 2011.
- [44] Facundo Mémoli and Guillermo Sapiro. A theoretical and computational framework for isometry invariant recognition of point cloud data. *Foundations of Computational Mathematics*, 5(3):313–347, 2005.
- [45] Michael I Miller, M Faisal Beg, Can Ceritoglu, and Craig Stark. Increasing the power of functional maps of the medial temporal lobe by using large deformation diffeomorphic metric mapping. *Proceedings of the National Academy of Sciences of the United States of America*, 102(27):9685–9690, 2005.
- [46] Michael I Miller, Alain Trouvé, and Laurent Younes. On the metrics and euler-lagrange equations of computational anatomy. *Annual review of biomedical engineering*, 4(1):375–405, 2002.
- [47] Michael I Miller, Alain Trouvé, and Laurent Younes. The metric spaces, euler equations, and normal geodesic image motions of computational anatomy. In *Image Processing, 2003. ICIP 2003. Proceedings. 2003 International Conference on*, volume 2, pages II–635. IEEE, 2003.
- [48] Michael I Miller, Alain Trouvé, and Laurent Younes. Geodesic shooting for computational anatomy. *Journal of mathematical imaging and vision*, 24(2):209–228, 2006.
- [49] Jan Modersitzki. *FAIR: Flexible Algorithms for Image Registration*. SIAM.
- [50] Marc Niethammer, Yang Huang, and François-Xavier Vialard. Geodesic regression for image time-series. In *Medical Image Computing and Computer-Assisted Intervention–MICCAI 2011*, pages 655–662. Springer, 2011.
- [51] Jorge Nocedal and Stephen J Wright. *Numerical Optimization, Second Edition*. Springer New York, 2006.
- [52] Danielle Pace, Marc Niethammer, and Aylward Stephen. Sliding geometries in deformable image registration. *LNCS*, 7029:141–148, 2011.
- [53] Anqi Qiu and Michael I Miller. Cortical hemisphere registration via large deformation diffeomorphic metric curve mapping. In *Medical Image Computing and Computer-Assisted Intervention–MICCAI 2007*, pages 186–193. Springer, 2007.
- [54] Anqi Qiu, Lei Wang, Laurent Younes, Michael P Harms, J Tilak Ratnanather, Michael I Miller, and John G Csernansky. Neuroanatomical asymmetry patterns in individuals with schizophrenia and their non-psychotic siblings. *Neuroimage*, 47(4):1221–1229, 2009.

- [55] Peter Risholm, Eigil Samset, Ion-Florin Talos, and William Wells. A non-rigid registration framework that accomodates resection and retraction information processing in medical imaging. *LNCS*, 5636:447–458, 2009.
- [56] Laurent Risser, F Vialard, Robin Wolz, Maria Murgasova, Darryl D Holm, and Daniel Rueckert. Simultaneous multi-scale registration using large deformation diffeomorphic metric mapping. *IEEE Transactions on Medical Imaging*, 30(10):1746–1759, 2011.
- [57] Laurent Risser, François-Xavier Vialard, Habib Y. Baluwala, and Julia A. Schnabel. Piecewise-diffeomorphic image registration: Application to the motion estimation between 3d {CT} lung images with sliding conditions. *Medical Image Analysis*, 17(2):182 – 193, 2013.
- [58] Alexander Schmidt-Richberg, Jan Ehrhardt, Rene Werner, and Heinz Handels. Slipping objects in image registration: Improved motion field estimation with direction-dependent regularization. *LNCS*, 5761:755–762, 2009.
- [59] Jean-Philippe Thirion. Image matching as a diffusion process: an analogy with maxwell’s demons. *Medical image analysis*, 2(3):243–260, 1998.
- [60] Emmanuel Trélat. *Contrôle optimal*. Mathématiques Concrètes. [Concrete Mathematics]. Vuibert, Paris, 2005. Théorie & applications. [Theory and applications].
- [61] Alain Trouvé. Diffeomorphisms groups and pattern matching in image analysis. *International Journal of Computer Vision*, 28(3):213–221, 1998.
- [62] Alain Trouvé, Stanley Durrleman, Xavier Pennec, and Nicholas Ayache. Sparse approximation of currents for statistics on curves and surfaces. In *Proceedings of MICCAI 2008*, 2008.
- [63] Marc Vaillant and Joan Glaunes. Surface Matching via Currents. In *Information Processing in Medical Imaging*, pages 381–392, 2005.
- [64] Tom Vercauteren, Xavier Pennec, Aymeric Perchant, and Nicholas Ayache. Non-parametric diffeomorphic image registration with the demons algorithm. In *Medical Image Computing and Computer-Assisted Intervention—MICCAI 2007*, pages 319–326. Springer, 2007.
- [65] Tom Vercauteren, Xavier Pennec, Aymeric Perchant, and Nicholas Ayache. Diffeomorphic demons: Efficient non-parametric image registration. *Neuroimage*, 45(1):S61–S72, 2009.
- [66] François-Xavier Vialard, Laurent Risser, Daniel Rueckert, and Colin J Cotter. Diffeomorphic 3D Image Registration via Geodesic Shooting Using an Efficient Adjoint Calculation. *International Journal of Computer Vision*, pages 1–13, 2011.
- [67] Camille Vidal, Joshua Hewitt, Stephanie Davis, Laurent Younes, Sanjay Jain, and Bruno Jedynek. Template registration with missing parts: Application to the segmentation of m. tuberculosis infected lungs. In *Biomedical Imaging: From Nano to Macro, 2009. ISBI’09. IEEE International Symposium on*, pages 718–721. IEEE, 2009.
- [68] Lei Wang, Faisal Beg, Tilak Ratnanather, Can Ceritoglu, Laurent Younes, John C Morris, John G Csernansky, and Michael I Miller. Large deformation diffeomorphism and momentum based hippocampal shape discrimination in dementia of the alzheimer type. *IEEE Transactions on Medical Imaging*, 26(4):462–470, 2007.
- [69] Yalin Wang, Wei Dai, Xianfeng Gu, Tony F Chan, Shing-Tung Yau, Arthur W Toga, and Paul M Thompson. Teichmüller shape space theory and its application to brain morphometry. In *Medical Image Computing and Computer-Assisted Intervention—MICCAI 2009*, pages 133–140. Springer, 2009.
- [70] Yalin Wang, Xianfeng Gu, Tony F Chan, Paul M Thompson, and Shing-Tung Yau. Intrinsic brain surface conformal mapping using a variational method. In *Medical Imaging 2004*, pages 241–252. International Society for Optics and Photonics, 2004.
- [71] Medha V Wyawahare, Pradeep M Patil, Hemant K Abhyankar, et al. Image registration techniques: an overview. *International Journal of Signal Processing, Image Processing and Pattern Recognition*, 2(3):11–28, 2009.
- [72] Laurent Younes. Jacobi fields in groups of diffeomorphisms and applications. *Quarterly of applied mathematics*, 65(1):113–134, 2007.
- [73] Laurent Younes. *Shapes and diffeomorphisms*, volume 171. Springer, 2010.
- [74] Laurent Younes. Spaces and manifolds of shapes in computer vision: An overview. *Image and Vision Computing*, 30(6):389–397, 2012.
- [75] Laurent Younes, Felipe Arrate, and Michael I Miller. Evolutions equations in computational anatomy. *Neuroimage*, 45(1):S40–S50, 2009.
- [76] Laurent Younes, J Tilak Ratnanather, Timothy Brown, Elizabeth Aylward, Peg Nopoulos, Hans Johnson, Vincent A Magnotta, Jane S Paulsen, Russell L Margolis, Roger L Albin, et al. Regionally selective atrophy of subcortical structures in prodromal hd as revealed by statistical shape analysis. *Human brain mapping*, 2012.
- [77] Wei Zeng and Xianfeng David Gu. Registration for 3d surfaces with large deformations using quasi-conformal curvature flow. In *Computer Vision and Pattern Recognition (CVPR), 2011 IEEE Conference*, pages 2457–2464. IEEE, 2011.
- [78] Yun Zeng, Chaohui Wang, Yang Wang, Xianfeng Gu, Dimitris Samaras, and Nikos Paragios. Dense non-rigid surface registration using high-order graph matching. In *Computer Vision and Pattern Recognition (CVPR), 2010 IEEE Conference*, pages 382–389. IEEE, 2010.
- [79] Jiangyang Zhang, Linda J Richards, Michael I Miller, Paul Yarowsky, Peter van Zijl, and Susumu Mori. Characterization of mouse brain and its development using diffusion tensor imaging and computational techniques. In *Engineering in Medicine and Biology Society, 2006. EMBS’06. 28th Annual International Conference of the IEEE*, pages 2252–2255. IEEE, 2006.
- [80] Darko Zikic, Ben Glocker, Oliver Kutter, Martin Groher, Nikos Komodakis, Ali Kamen, Nikos Paragios, and Nassir Navab. Linear intensity-based image registration by markov random fields and discrete optimization. *Medical image analysis*, 14(4):550–562, 2010.
- [81] Barbara Zitova and Jan Flusser. Image registration methods: a survey. *Image and Vision Computing*, 21(11):977–1000, 2003.

S. ARGUILLÈRE: CENTER FOR IMAGING SCIENCE AND DEPARTMENT OF APPLIED MATHEMATICS AND STATISTICS, JOHNS HOPKINS UNIVERSITY, 3400 N. CHARLES ST. BALTIMORE MD 21218

*E-mail address:* sarguillere@gmail.com

E. TRÉLAT: SORBONNE UNIVERSITÉS, UPMC UNIV PARIS 06, CNRS UMR 7598, LABORATOIRE JACQUES-LOUIS LIONS, AND INSTITUT UNIVERSITAIRE DE FRANCE, F-75005, PARIS, FRANCE.

*E-mail address:* emmanuel.trelat@upmc.fr

A. TROUVÉ: ECOLE NORMALE SUPÉRIEURE DE CACHAN, CENTRE DE MATHÉMATIQUES ET LEURS APPLICATIONS, CMLA, 61 AV. DU PDT WILSON, F-94235 CACHAN CEDEX, FRANCE

*E-mail address:* trouve@cmla.ens-cachan.fr

L. YOUNES: CENTER FOR IMAGING SCIENCE AND DEPARTMENT OF APPLIED MATHEMATICS AND STATISTICS, JOHNS HOPKINS UNIVERSITY, 3400 N. CHARLES ST. BALTIMORE MD 21218

*E-mail address:* laurent.younes@jhu.edu